Distinct subpopulations of DN1 thymocytes exhibit preferential αβ or γδ T lineage potential

Seungyoul Oh[1,2], Xin Liu[1], Sara Tomei[3,4], Mengxiao Luo[3,4], Jarrod Skinner[1], Stuart P. Berzins[5,6], Shalin H. Naik[3,4], Daniel H.D. Gray[3,4] & Mark M.W. Chong[1,2*]

1. St Vincent's Institute of Medical Research, Fitzroy, VIC, Australia
2. Department of Medicine (St Vincent's), University of Melbourne, Fitzroy, VIC, Australia
3. The Walter and Eliza Hall Institute of Medical Research, Melbourne, VIC, Australia
4. Department of Medical Biology, University of Melbourne, Melbourne, VIC, Australia
5. Department of Microbiology and Immunology, University of Melbourne, Melbourne, VIC, Australia
6. Institute of Innovation, Science and Sustainability, Federation University Australia, Ballarat, VIC, Australia

*Address correspondence to Mark M.W. Chong: mchong@svi.edu.au

Abstract

T cells are divided into the αβ and γδ lineages and both are though to differentiate in the thymus from uncommitted progenitor thymocytes. In this study, we employ single-cell RNA sequencing to reassemble *de novo* a model of early T cell development from individual $CD4^-CD8^-$ double negative and γδ thymocytes. We show that the earliest thymocyte stage, known as $CD4^-CD8^-$ double negative 1 (DN1), is comprised of a mixture of transcriptionally distinct subpopulations. Although not yet expressing definitive markers of αβ and γδ lineages, such as the lineage-defining T cell receptors, some DN subpopulations exhibit preferential development toward the αβ lineage while others exhibit preferential development toward the γδ lineage. Furthermore, specific γδ-primed DN1 subpopulations preferentially develop into IL-17 or IFNγ-producing γδ T cells. We show that DN1 subpopulations that only give rise to IL-17-producing γδ T cells already express many of the transcription factors associated with type 17 immune cell differentiation, while the DN1 subpopulations that give rise to IFNγ-producing γδ T cell already express transcription factors associated with type 1 immune cell differentiation. Thus, our findings suggest that lineage fate predetermination plays a role in γδ T cell development.

Introduction

T cells are divided into two principal lineages that are distinguished by the composition by their T cell receptors (TCRs) (Carpenter & Bosselut, 2010). Those that express an αβ TCR include conventional $CD4^+$ and $CD8^+$ T cells and these can be further divided into diverse subsets that have distinct immunologic functions (Harrington et al., 2005; Rothenberg, Moore, & Yui, 2008). T cells that express a γδ TCR are mainly divided into two subtypes defined by secretion of IL-17A or IFNγ. IL-17A-producing γδ T cells are important for immunity to intracellular bacteria, while IFNγ-producing γδ T cells are well-known for their anti-tumor function (Bai et al., 2017; Gao et al., 2016; Ribot, Lopes, & Silva-Santos, 2021).

T cell development occurs in the thymus, and it is thought that αβ and γδ T cells both arise from common progenitors that are seeded from the bone marrow (Ciofani & Zuniga-Pflucker, 2010; Taghon, Yui, Pant, Diamond, & Rothenberg, 2006). In mice, the earliest stages of T cell development are termed double-negative (DN) because they lack CD4 and CD8 expression. These are further subdivided into DN1 ($CD44^+CD25^-$), DN2 ($CD44^+CD25^+$), DN3 ($CD44^-CD25^+$) and DN4 ($CD44CD25^-$) stages. αβ and γδ development is thought to bifurcate at the DN2b>DN3 transition, when *TCRB/G/D* gene rearrangement occurs to generate a functional pre-TCR or γδ TCR (Ciofani, Knowles, Wiest, von Boehmer, & Zuniga-Pflucker, 2006; Fehling, Krotkova, Saint-Ruf, & von Boehmer, 1995; Kreslavsky, Gleimer, Garbe, & von Boehmer, 2010; Oh, Gray, & Chong, 2021). Evidence also suggests that effector outcomes of γδ T cells may also be determined in the thymus rather than in the periphery because the expression of IL-17A and IFNγ by mature cells correlates with Vγ chain usage. $V\gamma2^+$ γδ T cells tend to produce IL-17A while $V\gamma1^+$ γδ T cells tend to produce IFNγ (Fahl, Coffey, & Wiest, 2014; Narayan et al., 2012).

The prevailing model suggests that TCR signaling plays a deterministic role in lineage commitment and subsequent γδ effector differentiation (Munoz-Ruiz, Sumaria, Pennington, & Silva-Santos, 2017). Strong signals have been shown to activate ERK and induce EGR-ID3 and this appears to drive γδ differentiation, whereas

weak signals appear to promote an αβ fate (Hayes, Li, & Love, 2005; Lauritsen et al., 2009; Munoz-Ruiz et al., 2017). Additionally, weak TCR signaling may promote an IL-17A phenotype in γδ T cells, while strong signaling promotes an IFNγ phenotype (Sumaria, Grandjean, Silva-Santos, & Pennington, 2017). Evidence for an instructive role of the T-cell receptor in γδ T cell lineage commitment comes from a single-cell RNA sequencing (scRNA-seq) study that identified DN3 cells that expressed intermediate levels of γδ TCR in LAT deficient mice. LAT is an adaptor required for γδ TCR signaling and deficient thymocytes failed to turn on the transcriptional program associated with the γδ T cell lineage (Scaramuzzino et al., 2022). However, whether the lineage commitment is determined prior or at DN3 stage when TCR signaling remains unclear.

TCR signaling is unlikely to be the only determinant because a lack of Notch signaling at the DN2 stage compromises progression to DN3 and impairs αβ development but not γδ development (Tanigaki et al., 2004; Wolfer, Wilson, Nemir, MacDonald, & Radtke, 2002). How can the stage prior to the apparent γδ branching be compromised and yet γδ T cell development still proceed? The predetermination model proposes that αβ versus γδ T cell lineage commitment is determined by lineage specific factors prior to the onset of TCR gene rearrangement. Consequently, only those thymocytes that receive a corresponding signal via the stochastically expressed pre-TCR or γδTCR can further develop (Oh, Gray, & Chong, 2021; Scaramuzzino et al., 2022). Evidence suggest that this Notch-independence is at least partially due to the transcription factor ID3 because a weak TCR signal in cooperation with Notch signaling is sufficient to inhibit E-protein activity (Lauritsen et al., 2009). However, ID3 activity could explain the development of only a subset of γδ T cells. This murkiness surrounding the αβ versus γδ decision has arisen partly due to a lack of markers to define the development of thymocytes that have been selected to mature into γδ T cells (Pellicci, Koay, & Berzins, 2020). Together, these ambiguities raise the question as to whether the early stages of T cell development are really bipotent homogenous populations that can give rise to both αβ and γδ T cells. Emerging evidence in other developmental pathways suggests that progenitors can be heterogeneous with biases in lineage potential (Naik et al., 2013). In order to better understand the earliest stages of γδ lineage determination in the thymus, in this study, we perform

scRNA-seq of mouse DN and γδ thymocytes to determine the transcriptional heterogeneity at single-cell resolution and to assemble a model of early T cell development *de novo*.

Results

Differences in the kinetics of αβ versus γδ T cell development from DN1 thymocytes

We began by investigating the kinetics of αβ versus γδ T cell development in OP9-DL1 cultures, which supports the development of hematopoietic progenitors *in vitro* into either γδ T cells or αβ cells up to the $CD4^+CD8^+$ double positive (DP) stage (Holmes & Zuniga-Pflucker, 2009). Total DN1 ($CD44^+CD25^-Lin^-$) and DN2 ($CD44^+CD25^+Lin^-$) thymocytes were sorted from C57BL/6 mice and cocultured on OP9-DL1 cells. The cultures were then analyzed after 9-23d. DP cells were detected by CD8α (and CD4) expression while γδ cells were detected by TCRγδ expression (Fig EV1A-B).

While DN1 and DN2 thymocytes gave rise to both lineages, the development of DN1 thymocytes into γδ cells was more rapid compared to αβ cells. Starting from DN1 thymocytes, γδ cells were already present at 9d, with the percentage and cell number peaking at 12d, waning and then increasing again at 20d (Fig 1A and B). In contrast, αβ cells only started appearing after 14d and peaked at 20d. The earlier γδ peak suggests that γδ development is either simply more rapid than αβ development or that there may be different developmental pathways for the two lineages, with γδ cells potentially produced in two waves.

Unlike the discordant kinetics of the DN1 cultures, culturing DN2 thymocytes produced both αβ and γδ lineage cells from 9d and in similar proportions throughout (Fig 1A-B). γδ cells were produced at a consistently low frequency of 2-6%, while one-third to half were αβ cells at each timepoint. Given that DN2 thymocytes are only one stage along from DN1, the consistent rate of both αβ and γδ production suggests that γδ development is not simply more rapid.

If the αβ and γδ lineages develop independently, we might expect to see each lineage being derived from distinct DN1 thymocytes. To investigate this, we tagged individual DN1 thymocytes with unique genetic heritable barcodes (Naik et al., 2013) and tracked the propagation of these barcodes in OP9-DL1 cultures. If an αβ cell and γδ cell inherits the same barcode sequence, it means that they were derived from the same progenitor. CD8α^+ and TCR$\gamma\delta^+$ cells were sorted after 14d and 20d of culture and analyzed for barcode composition (Fig EV2A). While there was some overlap in barcode usage between the four populations, the barcode profiles were largely non-overlapping, with Pearson's correlations of $r<0.6$ for the first experiment (Fig 1D-E) and even lower in the second experiment (Fig EV2C-D). Together with the kinetic analysis, this suggest that the DN1 thymocytes may in fact be a heterogenous mixture consisting of distinct subpopulations that preferentially developed into either αβ cells or γδ cells.

A comprehensive transcriptional map of early T cell development at single-cell resolution

To better understand the potential heterogeneity of the early stages of T cell development, we next characterized the transcriptional landscape of DN and γδ thymocytes at single-cell resolution. Cells were sorted from the thymus of C57BL/6 mice for analysis by 10X scRNA-seq over three independent runs (Fig 2A-B and Appendix Table S1). The first run consisted of total DN and TCR$\gamma\delta^+$ cells, the second consisted only of DN1 and DN2 cells and the third involved sorting DN1+2, DN3 and TCR$\gamma\delta^+$ cells separately and mixing back together post-sort at a ratio of 55% to 30% to 15%, respectively (Fig 2A and Appendix Table S1). This was to ensure that a sufficient number of DN1 and DN2 cells were captured for high-resolution analysis that is not possible by analyzing total DN cells.

A total of 22,094 high quality cells passed quality control checks across the three 10X datasets. The three datasets were first integrated to assemble a global view of early T cell development. To recover biological distinction from these different replicates and minimize batch-associated variability, the pooled data was normalized using SCTransform. Following dimensional reduction, unsupervised clustering was performed using the first 12 principal components (PC). This identified 30 distinct clusters (Fig 2C), which were assigned to a

DN stage or mature γδ thymocytes based on the expression of canonical markers (Fig EV1A-B). High *Cd44* and *Il7r* expression but low T lineage gene expression, including *Il2ra, Tcf7, Cd24a, Notch1 and Bcl11b,* identified DN1 cells (Fig 2D). DN2 cells were identified by upregulation of T lineage genes and downregulation of *Il7r*. DN3 cells were identified by *Ptcra* and further upregulation of T lineage genes. Low *Cd8b1* and loss of *Il2ra* distinguished DN4 from DN3 cells (Fig 2D). High *Trdc, Id3, Sox13* and *Rorc* identified mature γδ thymocytes (Fig 2D). This analysis revealed that multiple distinct populations correspond to each of the canonical DN stages and consistent with recent T cell development studies (Spidale et al., 2018; Sagar et al., 2020; Scaramuzzino et al., 2022), this suggests that DN thymocytes are much more heterogenous than previously thought.

We also tested the effect of cell cycle gene expression on the clustering. Cell cycling scores were calculated from the integrated data and regressed using Seurat's built-in regression model (Fig EV3A-B). There was a slight variation in the number of output clusters, but we did not observe any biological variability that could be accounted for by cell cycle status, with the genetic profiles nearly identical between output with cell cycle genes left in or regressed out (Fig EV3C). Therefore, exclusion of cell cycle genes was not necessary for downstream analyses.

Trajectory analysis suggests that αβ and γδ T cell development occurs in parallel

To understand how the single cell transcriptomic map of DN and γδ thymocytes aligned with the established understanding of early T cell development, we reconstructed a developmental pathway *de novo* from the identified clusters by ordering the cells based on tracking gene expression in pseudotime analysis.

Pseudotime inference of the integrated data with Slingshot ordered the cells in the expected sequence from DN1 through to DN4, corresponding to αβ development (Street et al., 2018; Germain, 2002). There were also two branch points predicted, one corresponding to the γδ lineage branching from and remaining close to DN1 cells, and another branch point at DN2 that ended with a subpopulation of DN3 cells (Fig 3A).

We also performed pseudotime inference using Monocle 2 (Qiu et al., 2017), which assembled the cells along an asymmetric trajectory that divided into six states (Fig 3B). Each state was then analyzed for signature gene expression (Fig EV4) to assign the cells to the conventional DN development stages (Fig 3C-D). State 2 comprising DN1 and some DN2a cells, was identified as the starting point. State 3 corresponded to the main αβ pathway, with DN4 as the endpoint. States 5 and 6 terminated with DN3 and corresponded to β-selection failure (Fig 3B and D). State 1 corresponded to the γδ branch, and like Slingshot, Monocle 2 inferred that γδ cells develop directly from DN1 and remained transcriptionally close to each other. Interestingly, while *Rag* expression was highest in DN3 cells, which is expected, expression could already be detected in some DN1 cells (Fig 3E-F). Thus, trajectory analyses suggest that the γδ lineage decision may be much earlier than the current paradigm of branching at DN2b>DN3, which suggests at least a component of predetermination in γδ development (Fig EV1).

Extensive heterogeneity within DN1 and DN2 thymocytes

The trajectory analyses, as well as the OP9-DL1 kinetic studies, suggested that γδ T cell development might be occurring in parallel with αβ development, rather than branching off at the later DN2b>DN3 point. To better delineate the earlier stages of the developmental model, we analyzed the second 10X run that was performed specifically on DN1 and DN2 thymocytes. Unsupervised clustering of the 8,851 cells that pass quality control checks identified 26 distinct subpopulations (Fig 4A). Analysis for conventional stage marker genes identified eight DN1, five DN2a and 10 DN2b subpopulations (Fig 4A). There were also three small clusters of non-T cells consisting of doublets and B cells that, for simplicity, were excluded from downstream analysis. DN1s expressed high levels of progenitor markers, including *Hhex*, *Il7r* and *Cd44* but low levels of T-commitment markers, such as *Il2ra*, *Tcf7*, *Notch1*, *Cd24a* and *Myb* (Fig EV5A-B). Late T-lineage commitment genes, including *Rag1*, *Rag2*, *Notch3* and *Ptcra*, were used to separate DN2a and DN2b subpopulations (Fig EV5A-B). While heterogeneity in DN1 thymocytes was reported previously (Porritt et al., 2004), the degree of

heterogeneity among both DN1 and DN2 thymocytes was far more extensive than expected, which could be clearly seen by the differential expression of many marker genes (Fig EV5B).

Identification of novel cell surface markers for delineating DN1 and DN2 subpopulations

In order to study these novel subpopulations of DN1 and DN2 thymocytes, we needed to identify useful cell surface markers that could be used for flow cytometry. Differential expression analysis was performed to select features ($p<0.05$ and 2-fold difference) that were cross-referenced to GO terms for cell surface proteins (Appendix Fig S1A-B). We then tested commercial antibodies against these candidates. While not all antibodies produced a staining pattern consistent with mRNA expression levels, we were able to identify a minimal panel to delineate both DN1 and DN2 thymocytes.

The combination of five markers encoded by the genes *Cd24a*, *Kit*, *Bst2*, *Ly6a* and *Klrk1* distinguished the eight DN1 subpopulations (Fig 4B). CD24 and c-Kit was previously shown to separate DN1 thymocytes into five subpopulations, known as DN1a, DN1b, DN1c, DN1d and DN1e (Porritt et al., 2004). DN1a to DN1d each corresponded to a single cluster (Fig 4A). Bst2, Ly6a and Klrk1 were then used to delineate DN1e-1 to DN1e-4 (Fig 4C). The DN1a and DN1b subpopulations, together, correspond to the previously defined the earliest stage in T cell development, known as the early thymocyte progenitor, which are $CD44^{+}CD25^{-}$c-Kit^{+} cells (Porritt et al., 2004).

The pair of DN2a clusters 7/15 could not be separated by cell surface markers as well as the pairs of DN2b clusters 4/23, 9/13 and 8/19 due to very similar gene expression profiles. Thus, these cluster pairs were combined. The resulting 11 DN2 clusters were annotated as DN2a-1 to 4 and DN2b-1 to 7 based on the expression of genes encoded by *Thy1*, *Kit*, *Cd53*, *Ly6d* and *Cd3e* (Fig 4D-E).

Distinct DN1 subpopulations exhibit biases towards either the αβ or γδ lineage

The heterogeneity of the DN1 thymocytes could potentially represent different progenitors of αβ and γδ lineages, which would explain the early branch point inferred by pseudotime trajectory analyses (Fig 3A-C). To test this, we sorted the DN1 and DN2 subpopulations using our antibody panels and accessed their αβ versus γδ lineage outcomes in OP9-DL1 cultures after 14d and 20d (Fig 5A-F).

At 14d, we observed preferential αβ lineage differentiation in DN1a, DN1b and DN1c cultures, whereas DN1d and DN1e cultures only generated TCR$\gamma\delta^+$ cells (Fig 5A-C and Appendix Table S2). At 20d, there was a significant increase in the percentage and number of αβ cells produced from DN1a and DN1b, while DN1c had given rise to some γδ cells as well as αβ cells (Fig 5A-C and Appendix Table S3). DN1d and DN1e subpopulations continued to exhibit a bias toward the γδ lineage, with DN1e-1 and DN1e-2 producing the highest percentage and number of γδ T cell among DN1 subpopulations (Fig 5A-C and Appendix Table S2).

At 14d, all DN2b subpopulations and DN2a-1 produced a high percentage and number of αβ cells and few TCR$\gamma\delta^+$ cells, while the rest of DN2a subpopulations produced mostly TCR$\gamma\delta^+$ cells and few αβ lineage cells (Fig 5D-E, Appendix Fig S2 and Appendix Table S4). By day 20, all DN2 subpopulations had produced αβ lineage cells, while TCR$\gamma\delta^+$ cells had been lost from the DN2a cultures (Fig 5D-E, Appendix Fig S2 and Appendix Table S5). There was also a dramatic reduction in cell numbers in the DN2b cultures, which may be a result of the cells undergoing cell death after reaching the DP stage (Fig 5E).

We also tested the differentiation of select DN1 subpopulations in fetal thymic organ cultures (FTOCs). Like in the OP9-DL1 co-cultures, DN1b cells preferentially produced αβ cells, DN1c cells primary produced αβ cells and some γδ cells, while DN1d and DN1e-4 cells were biased toward the γδ lineage (Fig 5F). Thus, both OP9-DL1 and FTOC systems suggest that distinct DN1 subpopulations already exhibit a bias toward the γδ lineage. This again suggests that predetermination, prior to the onset of TCR gene rearrangement, is playing a role in γδ

development. However, there remains some flexibility because TCRγδ$^+$ cells can also differentiate from DN1c and DN2a subpopulations.

Gene expression analysis of DN1 subpopulations suggest potential relationships with distinct mature γδ subsets

Consistent with two group of γδ progenitors identified by Sagar and colleagues (Sagar et al., 2020), γδ thymocytes clearly segregate into two distinct but closely related clusters in our scRNA-seq dataset (Fig 2C). We therefore wanted to determine how these related to the different DN1 subpopulations. Firstly, differential expression analysis revealed substantial differences between two γδ clusters, with 93 genes expressed at significantly higher levels by the γδ-1 cluster while 117 genes were expressed at significantly higher levels by γδ-2 cluster (Fig 6A). Genes that were highly expressed by the γδ-1 cluster included *Gzma, Blk, Maf, Sox13, Etv5, Gata3, Ccr9, Rorc, Sox4, Tcf12, Lgals9, Cmak4* and *Bcl11b*, which are all associated with IL-17A-producing γδ T cell subset (Sagar et al., 2020). This suggests that the γδ-1 cluster is likely to be γδ thymocytes that go on to mature into the IL-17-producing subset, while the γδ-2 cluster are those that are likely to mature into the IFNγ producing γδ T cell subset. This is consistent with a previous study that suggested the eventual effector function of γδ T cells may already be acquired in the thymus (Sumaria et al., 2017). The unique transcriptional profiles of γδ-1 and γδ-2 thymocytes appears to be evidence of this.

Next, to investigate the relationship between the mature γδ thymocyte subpopulations and the DN1 subpopulations that differentiate into TCRγδ$^+$ cells, the DN1c, d and e subpopulations were analyzed for the expression of the 210 differentially genes that distinguished the two mature γδ thymocyte populations. This revealed a similar transcriptional profile between DN1d and γδ-1 thymocytes, while DN1c and all the DN1e subpopulations overlapped significantly with γδ-2 thymocytes (Fig 6B). However, there were also clearly differences between the DN1e subpopulations.

We then focused on transcription factors because they are regulators of gene expression and could potentially play key roles in the hardwiring γδ effector outcomes in DN1 thymocytes. *Sox13* was highly expressed by DN1d cells (Fig 6B), which was previously shown to be important for the differentiation of a subset of DN1 thymocytes into Tγδ17 cells (Spidale et al., 2018). Interestingly, DN1e subpopulations also express transcription factors associated with IL-17-producing γδ T cells. Notably, DN1e-1 and DN1e-2 cells expressed high levels of *Maf*, while *Gata3* was highly expressed by both DN1e-1 and DN1d cells (Fig 6B). We thus predicted that γδ effector outcomes could also already be pre-wired from the DN1 stage, with DN1d going on to develop into IL-17-producing cells and DN1e potentially producing both γδ effector subsets.

Different DN1 subpopulations can give rise to different γδ effector subsets

To determine if different DN1 subpopulations might differentiate into distinct effector γδ T cell subsets, the TCRγδ$^+$ cells that developed from the different DN1 subpopulations in OP9-DL1 co-cultures were analyzed for intracellular IL-17A and IFNγ expression and for expression of specific Vγ chains (Fig 7A). Cytokine production is highly associated with specific Vγ chain usage, with Vγ1$^+$ cells enriched for IFNγ and Vγ2$^+$ cells enriched for IL-17A production (Narayan et al., 2012; O'Brien & Born, 2010).

DN1c thymocytes generated both Vγ1$^+$ and Vγ2$^+$ cells, with only a low percentage of IFNγ expression by the Vγ1$^+$ cells (Fig 7B-D and Appendix Table S6). DN1d primarily produced Vγ2$^+$ cells that secreted IL-17A. Similarly, DN1e-1 and DN1e-2 were bias towards a Vγ2$^+$ IL-17A$^+$ γδ effector subset. On the other hand, only DN1e-3 and DN1e-4 exhibited the plasticity to generate both IL-17A and IFNγ producing cells (Fig 7B-D and Appendix Table S6). This suggests that effector subset predetermination may also be important in γδ development.

Discussion

Our understanding of the earliest events in T cell development has, until now, been complicated by two factors. First, it has been unclear if the earliest thymocytes constitute a truly bipotent homogenous population that can differentiate into both αβ and γδ lineages. Second, previous studies that analyzed whole populations by flow cytometry largely lacked the resolution to reveal the asynchronous development of rare subpopulations. Leveraging the power of scRNA-seq for rare cell type identification, our study has revealed the extensive heterogeneity within the early stages of T cell development. Consistent with previous reports (Spidale et al., 2018; Lavaert et al., 2020; Le et al., 2020), we identified the presence of rare and potentially biased precursors. We show that distinct DN1 subpopulations already exhibit a bias toward the γδ lineage. The DN1 (earliest) stage, instead of being an uncommitted T cell progenitor population, in fact consists of distinct subpopulations that appear to exhibit a developmental bias towards the αβ or γδ linage, even prior to the expression of the lineage-defining TCRs.

The concept that the early stages of T cell development may consist of distinct subpopulation has previously been considered. It was shown that DN1 thymocytes can be subdivided into five subpopulations (DN1a-e) based on CD24 and c-Kit expression (Porritt et al., 2004), while neonatal IL-17-producing cells were shown to develop from a subset of DN1d thymocytes that is determined by a cell intrinsic program prior to TCR signaling (Spidale et al., 2018). Despite these findings, the cellular heterogeneity of DN1 thymocytes, more broadly, and their lineage specification remained unclear, especially of the DN1e subpopulations. We have now defined eight DN1 subpopulations, including four novel DN1e subpopulations and showed that DN1a and DN1b are biased toward the αβ lineage whereas DN1d and DN1e subpopulations are biased toward the γδ lineage. This does not mean lineage commitment is determined in its entirety at this point because the progression from DN1 to fully mature γδ thymocytes almost certainly requires additional lineage-specific signals. While most DN1 subpopulations appeared to exhibit a predetermined fate, there remained some lineage flexibility. The fact that DN1e-3 and DN1e-4 cells can differentiate into both IL-17A and IFNγ-producing cells, and that DN1c and DN2a still displayed some γδ potential in addition to their dominant αβ outcome also suggest the importance of signals later in the developmental pathway.

Unlike αβ T cells, γδ T cells are thought to acquire their effector potential in the thymus rather than upon antigen exposure in secondary lymphoid organs (Ribot et al., 2009). A previous study showed that some IL-17-producing γδ T cells develop from a distinct subset of DN1 thymocytes (Spidale et al., 2018). Although none of the DN1 subpopulations expressed definitive markers of specific mature T cell populations, we observed substantial transcriptomic overlap between the IL-17-primed subpopulations with mature IL-17-expressing γδ thymocytes and between the IFNγ-primed subpopulations with mature IFNγ-expressing γδ thymocytes. Expression of key transcription factors was notable. We showed that DN1d thymocytes express many of transcription factors that are expressed by mature IL-17-producing γδ thymocytes but not IFNγ-producing thymocytes like *Bcl11b, Etv5, Sox13, Rcf7, Rorc and Maf*. Sox13 has previously be shown to be an important lineage determining factor for the neonatal IL-17A producing cells (Spidale et al., 2018). It is thought to act in concert with other transcription factors like *Bcl11b, Tcf7, Rorc* and *Maf* to specify the IL-17A-effector program in γδ T cells (Malhotra et al., 2013; Spidale et al., 2018).

While DN1e-1 and DN1e-2 were also biased towards a $V\gamma2^+$ IL-17A-producing γδ T cell fate, only DN1e-3 and DN1e-4 cell display the plasticity to also develop into $V\gamma1^+$ $IFN\gamma^+$ cells. This plasticity is likely to involve the differential expression of transcription factors that contribute to distinct effector fates. Although all four DN1e subpopulations expressed *Stat1*, which regulates IFNγ stimulated genes (Qiao et al., 2013), DN1e-1 and DN1e-2 also expressed *Maf*. cMaf is known to positively regulate IL-17A- producing γδ T cell development (Zuberbuehler et al., 2019), whereas a lack of cMaf expression by γδ T cells correlates with increased IFNγ expression (Gabrysova et al., 2018; Iwata et al., 2017; Zuberbuehler et al., 2019). Furthermore DN1e-1 cells were found to express *Gata3*, an important regulator of IFNγ expression (Yagi et al., 2010). The interplay between transcription factors may thus be key to lineage decisions. Thus, critical components of the IL-17 or IFNγ γδ T cell transcriptional programs appear to be already in place within distinct DN1 subpopulations, suggesting that predetermination contributes to γδ effector subset differentiation. Further analysis of chromatin

states and epigenetic mechanisms associated with these transcription factors will likely to be valuable to reveal the intricacies of the regulatory cascades that drive the different γδ effector outcomes.

Current models for the αβ versus γδ lineage decision frequently center on the role of TCR signals at the DN2b>3 stage. The evidence for a role of differing TCR signals comes from studies that have employed genetic mouse models to manipulate TCR signaling at the DN3 stage. These revealed that strong signals activate the ERK-EGR-ID3 pathway to drive γδ T cell differentiation, whereas a weak signal promotes the αβ fate (Hayes et al., 2005; Lauritsen et al., 2009; Munoz-Ruiz et al., 2017). TCRγδ signaling is also thought to play a role in subsequent γδ T cell effector differentiation (Munoz-Ruiz et al., 2017). Weak TCR signaling appears to promote an IL-17A effector phenotype, while strong signaling promotes IFNγ phenotype (Sumaria et al., 2017). However, it is still unclear whether TCR signal strength is dependent on instructive extrinsic signals or simply a result of stochastic selection of TCR chains. The instructive model proposes that TCRγδ signals competes with pre-TCR(β) signals and the lineage decision is determined by cell specific interactions that activate key transcription factors, which in turn instructs gene expression program (Carpenter & Bosselut, 2010). In contrast, the stochastic selective model postulates that lineage commitment is determined prior to the onset of TCR gene rearrangement, and those thymocytes that receives appropriate TCR signaling that matches their hardwired identity further progress along the αβ versus γδ lineage and differentiate into a specific subset of γδ T cells (Scaramuzzino et al., 2022). Indeed, Scaramuzzino and colleagues showed that TCR signaling clearly has a role in γδ lineage maturation because LAT-deficient DN3 cells that express a γδ TCR are unable to complete the activation of the γδ T cell lineage, including expression of *Sox13*, *Maf*, and *Cpa3*. The way we interpret our study with these previous findings is that the αβ versus γδ lineage decision (even down to the level of effector outcomes of γδ T cells) is at least partially hardwired from the DN1 stage of T cell development, but appropriate TCR signalling may still important for lineage commitment and maturation of the lineages.

Our finding of highly heterogenous DN1 and DN2 subpopulations highlights the concept that progenitor populations may not actually be multi/bipotent cells but in fact may be a grouping of lineage-primed cells at a similarly early stage in differentiation. On the surface, they may lack lineage defining markers and they are similar enough to appear to constitute a population, but individually, these cells have unique transcriptional programs that already specify a lineage-fate. Such heterogeneity in progenitor populations is increasingly being reported. For example, lymphoid-primed multipotent progenitors in the bone marrow also appear to exhibit substantial restriction to specific lineage fates (Naik et al., 2013). More specifically, myeloid progenitors can be divided into subpopulations that are primed towards neutrophil, basophil, eosinophil, monocyte, dendritic cell, erythrocyte or megakaryocyte fate (Paul et al., 2016). Clearly, our understanding of lineage determination, both of T cells and the immune system more broadly, remains incomplete and much remains to be elucidate. Nevertheless, our findings have provided new evidence for a role of lineage pre-determination in αβ versus γδ T cell development.

Materials and Methods

Mice and thymocyte preparations

Thymuses was harvested from C57BL/6 mice at around 6 weeks of age. All experiments were approved by the St Vincent's Hospital Animal Ethics Committee and performed under the Australian code for the care and use of animals for scientific purposes.

Total thymocytes were obtained by crushing the thymus through a metal sieve to generate a single cell suspension. The cells were washed with PBS and filtered through a 70 μm sieve to remove any clumps. $CD4^+$ and $CD8^+$ expressing thymocytes were depleted using anti-CD4 and CD8 magnetic-activated cell-sorting (MACS) beads (Miltenyi Biotec), according to the manufacturer's instructions. The depleted thymocyte preparation was stained with surface antibodies for sorting on a FACSAria (BD Biosciences).

Flow cytometry

For the analysis of cell surface phenotype, the cells were simply stained with antibodies. For the analysis of intracellular cytokine expression, cells were first restimulated *in vitro* with 50ng/mL phorbol 12-myristate 13-acetate (PMA) + 2 μg/mL ionomycin (both Sigma-Aldrich) in the presence of Monensin (BD Biosciences) at 37°C for 2.5h before staining with cell surface antibodies. The cells were then fixed with the Intracellular Fixation and Permeabilization buffer set (eBioscience) and stained with antibodies against cytokines. All antibodies were purchased from eBiosciences or BD Biosciences. Flow cytometry data were then acquired on a BD LSR Fortessa III (BD Biosciences) and analyzed with FlowJo software v10.7.0 (Treestar). When only analyzing cell surface phenotype, dead cells were excluded by DAPI. For intercellular cytokine analyses the cells were not stained with DAPI but were gated on live cells determined by size.

OP9-DL1 co-cultures

Thymocyte subpopulations for interest were purified by MACS depletion and cell sorting then plated onto OP9-DL1 monolayers (Holmes & Zuniga-Pflucker, 2009). The OP9-DL1 cells were inactivate with Mitomycin C (Stem Cell) immediately prior to use. 5×10^2 to 3×10^3 sorted thymocytes were seeded per well of a 96-well plate in aMEM (Life Technologies) supplemented with 20% FCS (Bovogen Biologicals), penicillin/streptomycin/gentamycin (Gibco), 2ng/mL murine IL-7 (Peprotech) and 5ng/mL human FLT3L (Peprotech) and were incubated at 37°C and 5% CO_2. The media was refreshed every 2d and freshly inactivated OP9-DL1 cells were added every 4d. The cells were analyzed by flow cytometry after 9-26d of culture.

Fetal thymic organ culture (FTOC)

Fetal thymic lobes were isolated from embryos at gestational 14d following timed pregnancies of C57BL/6 female mice. They were cultured for 5-6d on 0.8mm isopore membranes (Millipore) atop surgical gelfoam sponge (Ferrosan Medical Devices) soaked in RPMI-1640 (Sigma) supplemented with 10% FCS (Bovogen Biologicals), 20mM HEPES (Sigma-Aldrich), 50mM 2-mercaptoethanol (Sigma) and 1.35mM 2'-deoxygyanosine (dGuo, Sigma) to deplete endogenous thymocytes. The depleted thymic lobes were then transferred onto new sponges soaked in fresh media with supplements but without dGuo for 2d before

repopulation with thymocyte progenitors. To repopulate thymic lobes, they were placed in 20mL hanging drop cultures on Terasaki plates (Sigma-Aldrich) containing 5×10^2 to 2×10^3 sorted thymocytes for 24h before returning to fresh sponges. The media was refreshed every 3-4d. Single cell suspensions of the thymic lobes were generated by passing through a 70mm sieve for analysis by flow cytometry.

Barcode transduction

Sorted total DN1 thymocytes were pre-cultured on OP9-DL1 for 24h. The cells were then transduced with barcode lentivirus library(Naik et al., 2013) in StemSpan medium (Stem Cell Technologies) by centrifugation at 900 ×g for 1.5h at room temp. A viral titer pre-determined to give 10% transduction efficiency was used to ensure that the cells are not transduced with multiple barcodes. 2ng/mL murine IL-7 and 5ng/mL human FLT3L was then added to each well and the cells were returned to the incubator. The following day, fresh αMEM with supplements was added. αβ (CD90.2$^+$ CD8α$^+$ TCRγδ$^-$) and γδ (CD90.2$^+$ CD8α$^-$ TCRγδ$^+$) lineage cells were sorted after 14d and 20d OP9-DL1 co-culture.

Barcode amplification and sequencing

Barcode library construction was performed as described previously(Naik et al., 2013). The cells were lysed in 0.5mg/ml Proteinase K (Invitrogen) in Direct PCR Lysis Buffer (Viagen) at 55° C for 2h. The Proteinase K was then inactivated at 85°C for 30min and 95° C for 5min. The lysate was split into 2 wells for technical replicate PCRs. A first round of PCR was performed using 1× Standard-Taq magnesium free reaction buffer pack (NEB) with 2 mM MgCl2 (NEB), 0.2mM dNTPs (made in house), 0.5μM TopLiB forward primer (TGCTGCCGTCAACTAGAACA) and 0.5μM of BotLiB reverse primer (GATCTCGAATCAGGCGCTTA) for 32 cycles (1 cycle at 95 °C for
5min, 30 cycles at 95°C for 15sec, 57.2°C for 15sec and 72°C for 15sec followed by 1
cycle at 72°C for 10min). A second round of PCR was then performed to add different Illumina index to each sample by amplifying the first round PCR product with a sample specific Illumina forward index primer and a common Illumina reverse index primer for 32 cycles (1 cycle at 95°C for 5min, 30 cycles at 95°C for 15sec,

57.2°C for 15sec and 72°C for 15sec followed by 1 cycle at 72°C for 10min). An aliquot of the PCR product was run on a 2% agarose gel to check for barcode amplification, then the samples were pooled and the DNA was cleaned using NucleoMag SPRI beads (Machery-Nagel). A 75-cycle sequencing run was performed on a NextSeq instrument (Illumina).

Cellular barcode data processing and analysis

The data was demultiplexed and aligned to the reference barcode library using *processAmplicons* function from edgeR package (Robinson, McCarthy, & Smyth, 2010). The barcode counts were then processed in the following steps: 1) barcodes with 0 read counts in all sample/cell types were excluded from the analysis; 2) Barcodes that were detected in the water control were also removed from the analysis; 3) The read count between technical replicates of the same sample was averaged and the total read count in each sample was then normalized to 100%.

t-distributed stochastic neighbor embedding (t-SNE) was used to the cluster the normalized barcode profiles and visualize any lineage biases of individual barcodes. DBSCAN (version 1.1-8) was then used to classify barcodes based on their corresponding t-SNE coordinates. Heatmaps were plotted to visualize lineage output of barcodes that were identified by transforming the normalized reads value for each barcode using logarithmic transformation. Two-tailed Pearson's correlation analysis with 95% confidence interval was calculated to determine the correlation between each lineage outcomes using Prism v9 (GraphPad).

Single-cell RNA sequencing

Sorted thymocytes were counted and checked for viability, then loaded onto the 10X Chromium platform (10X Genomics) for scRNA-seq library construction using the Single Cell V2 or V3.1 Reagent Kit according to the manufacturer's instructions. Libraries were sequenced using 150-cycle/150bp-reads NextSeq500 (Illumina) or 300-cycle/150bp-reads Novaseq (Illumina). Sequencing files were demultiplexed and aligned to *Mus musculus*

transcriptome reference (mm10), and count matrix was extracted using CellRanger Single Cell software v2.1.1 or v4.0.0 (10X Genomics) (Zheng et al., 2017) (Supplementary Table 1).

The Illumina sequencing output was pre-processed with Seurat (v2.3 or v.3.2.2) on R (v3.6.3 and 4.1.0). Cells with <500 genes, >5000 genes or >7% mitochondria gene expression were filtered out as low-quality cells. Following normalization and removal of confounders, highly variable genes were identified and selected using VST selection method (Zwiener, Frisch, & Binder, 2014). Unsupervised linear principal component analysis (PCA) was performed on these highly variable genes to grouped them into 20 principal components. Cell clustering was implemented using the number of components that retain >90% of variance of gene expression in the data (stated in Supplementary Table 1).

DoubletFinder (v2.0.3) was applied to remove likely sequencing doublets before downstream analyses (McGinnis, Murrow, & Gartner, 2019). The expected number of doublets was calculated as 0.75% of every 1,000 targeted cells of recovery. The remaining cells were re-clustered and were visualized with t-SNE or uniform manifold approximation and projection (UMAP) dimensional reduction with a resolution of 2.0 (Table S1). Differential expression between subclusters was carried out using FindAllMarkers function, with default parameters; differentially expressed genes with adjusted *p*-value <0.05 and fold change >0.5 or <-0.5 (log2FC) were considered unless otherwise stated. The heatmaps was generated using function DoHeatmap. Hierarchical clustering heatmaps were generated with the R package ComplexHeatmap (v2.8.0) using Euclidean distance measures (Gu, Eils, & Schlesner, 2016).

Cell cycle genes specific to either the G1, S, G2M stages was used to perform cell cycle scoring and assign cells to their respective stage of the cell cycle (Macosko et al., 2015). Cell cycle genes were regressed using Seurat's built-in regression model.

Merging of multiple scRNA-seq datasets

To compare cell types and proportions across three independent sequencing runs, the datasets were integrated as described at https://satijalab.org/seurat/archive/v3.0/integration.html (Stuart et al., 2019). The Seurat package (v.3.2.2) was used to assemble multiple distinct scRNA-seq datasets into an integrated dataset and cell cycling scores were calculated. To remove technical variability, the datasets were pre-processed and normalized using SCTransform (Hafemeister & Satija, 2019). To correct for experimental batch effect, integration anchors were identified between the experiments then merged using canonical correlation analysis. Linear dimensional reduction was applied and principal components that retain >90% of variance of gene expression in the data were included for downstream analysis. Unsupervised clustering was implemented on the integrated data and clustered the cells using a resolution of 2.0.

Pseudotime trajectory construction

Filtered 10X data was imported into Monocle 2 by generating a cell dataset from the raw counts slot of the Seurat object. Cells were ordered into a branch pseudotime trajectory according to the procedure recommended in the Monocle 2 documentation (Qiu et al., 2017). The highly variable genes identified by Seurat were chosen as ordering genes to recover pseudospatial trajectories using the setOrderingFilter, reduceDimension and orderCells functions in Monocle 2 using default parameters. Differential expression between pseudotime states were determined using the Seurat function FindAllMarkers.

Slingshot trajectory construction

Cluster information from merged 10X dataset were used as input for Slingshot package (v2.0.0) to infer cell trajectory (Street et al., 2018). Default parameters was applied and DN1b was set as the starting point for the minimum spanning tree. The previously generated UMAP clustering from the integrated data was set as the cellular embedding on which Slingshot performed trajectory inference computation.

GO term enrichment analysis

The biomaRt package (v3.13) was loaded from the Bioconductor using R studio(Amezquita et al., 2020). The Gene Ontology (GO) terms Cell surface markers (0009986) and Transcription factors (0003700, 0008134, 0140110) were obtained from 'mmusculus_gene_ensembl' and applied to the input (differentially expressed) gene lists. Gene ontology enrichment analysis for GO Biological Process was conducted using ShinyGo (v0.66) (Ge, Jung, & Yao, 2020).

Statistical analysis

Statistical testing was performed with one-way analyses of variance (ANOVA) using Prism v9 (GraphPad). *P* values are shown as * < 0.05, ** < 0.01, *** < 0.001, and **** < 0.0001 where each statistical significance was found, and all data are represented as means ± S.E.M.

Data availability

All scRNA-seq datasets have been deposited in the NCBI Gene Expression Omnibus repository under accession number GSE188913.

Acknowledgments

We thank Lucy Kloboucnik in the St Vincent's Hospital Melbourne's BioResources Centre for expert animal husbandry, and Anthony Di Carluccio from St Vincent's Institute's Cytometry Facility and Casey Anttila from Walter and Eliza Hall Institute's Cytometry Facility for assistance with cell sorting and the scRNA-seq libraries. We also thank Dr David Izon (St Vincent's Institute) for the OP9-DL1 cell line, who originally obtained them from Dr Juan Carlos Zúñiga-Pflücker (University of Toronto).

This work was supported by grants and fellowships from the National Health and Medical Research Council, Australia (1078763, 1090236, 1145888 and 1158024 to D.H.D.G. and 1079586, 1117154, 1122384 and 1122395 to M.M.W.C.), Cancer Council Victoria (1102104 to D.H.D.G.), Diabetes Australia (Y20G-CHOM to

M.M.W.C.) and U.S. Department of Defense (W81XWH-19-1-0728 to M.M.W.C.) and the Victorian State Government Operational Infrastructure Support and the Independent Research Institutes Infrastructure Support Scheme of the National Health and Medical Research Council, Australia.

Competing interests

The authors declare that they have no competing interests.

References

Amezquita, R. A., Lun, A. T. L., Becht, E., Carey, V. J., Carpp, L. N., Geistlinger, L., . . . Hicks, S. C. (2020). Orchestrating single-cell analysis with Bioconductor. *Nat Methods, 17*(2), 137-145. doi:10.1038/s41592-019-0654-x

Bai, H., Gao, X., Zhao, L., Peng, Y., Yang, J., Qiao, S., . . . Yang, X. (2017). Respective IL-17A production by gammadelta T and Th17 cells and its implication in host defense against chlamydial lung infection. *Cell Mol Immunol, 14*(10), 850-861. doi:10.1038/cmi.2016.53

Carpenter, A. C., & Bosselut, R. (2010). Decision checkpoints in the thymus. *Nat Immunol, 11*(8), 666-673. doi:10.1038/ni.1887

Ciofani, M., Knowles, G. C., Wiest, D. L., von Boehmer, H., & Zuniga-Pflucker, J. C. (2006). Stage-specific and differential notch dependency at the alphabeta and gammadelta T lineage bifurcation. *Immunity, 25*(1), 105-116. doi:10.1016/j.immuni.2006.05.010

Ciofani, M., & Zuniga-Pflucker, J. C. (2010). Determining gammadelta versus alphass T cell development. *Nat Rev Immunol, 10*(9), 657-663. doi:10.1038/nri2820

Fahl, S. P., Coffey, F., & Wiest, D. L. (2014). Origins of gammadelta T cell effector subsets: a riddle wrapped in an enigma. *J Immunol, 193*(9), 4289-4294. doi:10.4049/jimmunol.1401813

Fehling, H. J., Krotkova, A., Saint-Ruf, C., & von Boehmer, H. (1995). Crucial role of the pre-T-cell receptor alpha gene in development of alpha beta but not gamma delta T cells. *Nature, 375*(6534), 795-798. doi:10.1038/375795a0

Gabrysova, L., Alvarez-Martinez, M., Luisier, R., Cox, L. S., Sodenkamp, J., Hosking, C., . . . O'Garra, A. (2018). c-Maf controls immune responses by regulating disease-specific gene networks and repressing IL-2 in CD4(+) T cells. *Nat Immunol, 19*(5), 497-507. doi:10.1038/s41590-018-0083-5

Gao, J., Shi, L. Z., Zhao, H., Chen, J., Xiong, L., He, Q., . . . Sharma, P. (2016). Loss of IFN-gamma Pathway Genes in Tumor Cells as a Mechanism of Resistance to Anti-CTLA-4 Therapy. *Cell, 167*(2), 397-404 e399. doi:10.1016/j.cell.2016.08.069

Ge, S. X., Jung, D., & Yao, R. (2020). ShinyGO: a graphical gene-set enrichment tool for animals and plants. *Bioinformatics, 36*(8), 2628-2629. doi:10.1093/bioinformatics/btz931

Germain, R. N. (2002). T-cell development and the CD4-CD8 lineage decision. *Nat Rev Immunol, 2*(5), 309-322. doi:10.1038/nri798

Gu, Z., Eils, R., & Schlesner, M. (2016). Complex heatmaps reveal patterns and correlations in multidimensional genomic data. *Bioinformatics, 32*(18), 2847-2849. doi:10.1093/bioinformatics/btw313

Hafemeister, C., & Satija, R. (2019). Normalization and variance stabilization of single-cell RNA-seq data using regularized negative binomial regression. *Genome Biol, 20*(1), 296. doi:10.1186/s13059-019-1874-1

Harrington, L. E., Hatton, R. D., Mangan, P. R., Turner, H., Murphy, T. L., Murphy, K. M., & Weaver, C. T. (2005). Interleukin 17-producing CD4+ effector T cells develop via a lineage distinct from the T helper type 1 and 2 lineages. *Nat Immunol, 6*(11), 1123-1132. doi:10.1038/ni1254

Hayes, S. M., Li, L., & Love, P. E. (2005). TCR signal strength influences alphabeta/gammadelta lineage fate. *Immunity, 22*(5), 583-593. doi:10.1016/j.immuni.2005.03.014

Holmes, R., & Zuniga-Pflucker, J. C. (2009). The OP9-DL1 system: generation of T-lymphocytes from embryonic or hematopoietic stem cells in vitro. *Cold Spring Harb Protoc, 2009*(2), pdb prot5156. doi:10.1101/pdb.prot5156

Iwata, S., Mikami, Y., Sun, H. W., Brooks, S. R., Jankovic, D., Hirahara, K., . . . Kanno, Y. (2017). The Transcription Factor T-bet Limits Amplification of Type I IFN Transcriptome and Circuitry in T Helper 1 Cells. *Immunity*, *46*(6), 983-991 e984. doi:10.1016/j.immuni.2017.05.005

Kreslavsky, T., Gleimer, M., Garbe, A. I., & von Boehmer, H. (2010). alphabeta versus gammadelta fate choice: counting the T-cell lineages at the branch point. *Immunol Rev*, *238*(1), 169-181. doi:10.1111/j.1600-065X.2010.00947.x

Lauritsen, J. P., Wong, G. W., Lee, S. Y., Lefebvre, J. M., Ciofani, M., Rhodes, M., . . . Wiest, D. L. (2009). Marked induction of the helix-loop-helix protein Id3 promotes the gammadelta T cell fate and renders their functional maturation Notch independent. *Immunity*, *31*(4), 565-575. doi:10.1016/j.immuni.2009.07.010

Lavaert, M., Liang, K. L., Vandamme, N., Park, J. E., Roels, J., Kowalczyk, M. S., . . . Taghon, T. (2020). Integrated scRNA-Seq Identifies Human Postnatal Thymus Seeding Progenitors and Regulatory Dynamics of Differentiating Immature Thymocytes. *Immunity*, *52*(6), 1088-1104 e1086. doi:10.1016/j.immuni.2020.03.019

Le, J., Park, J. E., Ha, V. L., Luong, A., Branciamore, S., Rodin, A. S., . . . Parekh, C. (2020). Single-Cell RNA-Seq Mapping of Human Thymopoiesis Reveals Lineage Specification Trajectories and a Commitment Spectrum in T Cell Development. *Immunity*, *52*(6), 1105-1118 e1109. doi:10.1016/j.immuni.2020.05.010

Macosko, E. Z., Basu, A., Satija, R., Nemesh, J., Shekhar, K., Goldman, M., . . . McCarroll, S. A. (2015). Highly Parallel Genome-wide Expression Profiling of Individual Cells Using Nanoliter Droplets. *Cell*, *161*(5), 1202-1214. doi:10.1016/j.cell.2015.05.002

Malhotra, N., Narayan, K., Cho, O. H., Sylvia, K. E., Yin, C., Melichar, H., . . . Immunological Genome Project, C. (2013). A network of high-mobility group box transcription factors programs innate interleukin-17 production. *Immunity*, *38*(4), 681-693. doi:10.1016/j.immuni.2013.01.010

McGinnis, C. S., Murrow, L. M., & Gartner, Z. J. (2019). DoubletFinder: Doublet Detection in Single-Cell RNA Sequencing Data Using Artificial Nearest Neighbors. *Cell Syst, 8*(4), 329-337 e324. doi:10.1016/j.cels.2019.03.003

Munoz-Ruiz, M., Sumaria, N., Pennington, D. J., & Silva-Santos, B. (2017). Thymic Determinants of gammadelta T Cell Differentiation. *Trends Immunol, 38*(5), 336-344. doi:10.1016/j.it.2017.01.007

Naik, S. H., Perie, L., Swart, E., Gerlach, C., van Rooij, N., de Boer, R. J., & Schumacher, T. N. (2013). Diverse and heritable lineage imprinting of early haematopoietic progenitors. *Nature, 496*(7444), 229-232. doi:10.1038/nature12013

Narayan, K., Sylvia, K. E., Malhotra, N., Yin, C. C., Martens, G., Vallerskog, T., . . . Immunological Genome Project, C. (2012). Intrathymic programming of effector fates in three molecularly distinct gammadelta T cell subtypes. *Nat Immunol, 13*(5), 511-518. doi:10.1038/ni.2247

O'Brien, R. L., & Born, W. K. (2010). gammadelta T cell subsets: a link between TCR and function? *Semin Immunol, 22*(4), 193-198. doi:10.1016/j.smim.2010.03.006

Oh, S., Gray, D. H. D., & Chong, M. M. W. (2021). Single-Cell RNA Sequencing Approaches for Tracing T Cell Development. *The Journal of Immunology, 207*(2), 363-370. doi:10.4049/jimmunol.2100408

Paul, F., Arkin, Y., Giladi, A., Jaitin, D. A., Kenigsberg, E., Keren-Shaul, H., . . . Amit, I. (2016). Transcriptional Heterogeneity and Lineage Commitment in Myeloid Progenitors. *Cell, 164*(1-2), 325. doi:10.1016/j.cell.2015.12.046

Pellicci, D. G., Koay, H. F., & Berzins, S. P. (2020). Thymic development of unconventional T cells: how NKT cells, MAIT cells and gammadelta T cells emerge. *Nat Rev Immunol, 20*(12), 756-770. doi:10.1038/s41577-020-0345-y

Porritt, H. E., Rumfelt, L. L., Tabrizifard, S., Schmitt, T. M., Zuniga-Pflucker, J. C., & Petrie, H. T. (2004). Heterogeneity among DN1 prothymocytes reveals multiple progenitors with different capacities to generate T cell and non-T cell lineages. *Immunity, 20*(6), 735-745. doi:10.1016/j.immuni.2004.05.004

Qiao, Y., Giannopoulou, E. G., Chan, C. H., Park, S. H., Gong, S., Chen, J., . . . Ivashkiv, L. B. (2013). Synergistic activation of inflammatory cytokine genes by interferon-gamma-induced chromatin

remodeling and toll-like receptor signaling. *Immunity, 39*(3), 454-469. doi:10.1016/j.immuni.2013.08.009

Qiu, X., Mao, Q., Tang, Y., Wang, L., Chawla, R., Pliner, H. A., & Trapnell, C. (2017). Reversed graph embedding resolves complex single-cell trajectories. *Nat Methods, 14*(10), 979-982. doi:10.1038/nmeth.4402

Ribot, J. C., deBarros, A., Pang, D. J., Neves, J. F., Peperzak, V., Roberts, S. J., . . . Silva-Santos, B. (2009). CD27 is a thymic determinant of the balance between interferon-gamma- and interleukin 17-producing gammadelta T cell subsets. *Nat Immunol, 10*(4), 427-436. doi:10.1038/ni.1717

Ribot, J. C., Lopes, N., & Silva-Santos, B. (2021). gammadelta T cells in tissue physiology and surveillance. *Nat Rev Immunol, 21*(4), 221-232. doi:10.1038/s41577-020-00452-4

Robinson, M. D., McCarthy, D. J., & Smyth, G. K. (2010). edgeR: a Bioconductor package for differential expression analysis of digital gene expression data. *Bioinformatics, 26*(1), 139-140. doi:10.1093/bioinformatics/btp616

Rothenberg, E. V., Moore, J. E., & Yui, M. A. (2008). Launching the T-cell-lineage developmental programme. *Nat Rev Immunol, 8*(1), 9-21. doi:10.1038/nri2232

Sagar, Pokrovskii, M., Herman, J. S., Naik, S., Sock, E., Zeis, P., . . . Grun, D. (2020). Deciphering the regulatory landscape of fetal and adult gammadelta T-cell development at single-cell resolution. *EMBO J, 39*(13), e104159. doi:10.15252/embj.2019104159

Scaramuzzino, S., Potier, D., Ordioni, R., Grenot, P., Payet-Bornet, D., Luche, H., & Malissen, B. (2022). Single-cell transcriptomics uncovers an instructive T-cell receptor role in adult gammadelta T-cell lineage commitment. *EMBO J, 41*(5), e110023. doi:10.15252/embj.2021110023

Spidale, N. A., Sylvia, K., Narayan, K., Miu, B., Frascoli, M., Melichar, H. J., . . . Kang, J. (2018). Interleukin-17-Producing gammadelta T Cells Originate from SOX13(+) Progenitors that Are Independent of gammadeltaTCR Signaling. *Immunity, 49*(5), 857-872 e855. doi:10.1016/j.immuni.2018.09.010

Street, K., Risso, D., Fletcher, R. B., Das, D., Ngai, J., Yosef, N., . . . Dudoit, S. (2018). Slingshot: cell lineage and pseudotime inference for single-cell transcriptomics. *BMC Genomics*, *19*(1), 477. doi:10.1186/s12864-018-4772-0

Stuart, T., Butler, A., Hoffman, P., Hafemeister, C., Papalexi, E., Mauck, W. M., 3rd, . . . Satija, R. (2019). Comprehensive Integration of Single-Cell Data. *Cell*, *177*(7), 1888-1902 e1821. doi:10.1016/j.cell.2019.05.031

Sumaria, N., Grandjean, C. L., Silva-Santos, B., & Pennington, D. J. (2017). Strong TCRgammadelta Signaling Prohibits Thymic Development of IL-17A-Secreting gammadelta T Cells. *Cell Rep*, *19*(12), 2469-2476. doi:10.1016/j.celrep.2017.05.071

Taghon, T., Yui, M. A., Pant, R., Diamond, R. A., & Rothenberg, E. V. (2006). Developmental and molecular characterization of emerging beta- and gammadelta-selected pre-T cells in the adult mouse thymus. *Immunity*, *24*(1), 53-64. doi:10.1016/j.immuni.2005.11.012

Tanigaki, K., Tsuji, M., Yamamoto, N., Han, H., Tsukada, J., Inoue, H., . . . Honjo, T. (2004). Regulation of alphabeta/gammadelta T cell lineage commitment and peripheral T cell responses by Notch/RBP-J signaling. *Immunity*, *20*(5), 611-622. doi:10.1016/s1074-7613(04)00109-8

Wolfer, A., Wilson, A., Nemir, M., MacDonald, H. R., & Radtke, F. (2002). Inactivation of Notch1 impairs VDJbeta rearrangement and allows pre-TCR-independent survival of early alpha beta Lineage Thymocytes. *Immunity*, *16*(6), 869-879. doi:10.1016/s1074-7613(02)00330-8

Yagi, R., Junttila, I. S., Wei, G., Urban, J. F., Jr., Zhao, K., Paul, W. E., & Zhu, J. (2010). The transcription factor GATA3 actively represses RUNX3 protein-regulated production of interferon-gamma. *Immunity*, *32*(4), 507-517. doi:10.1016/j.immuni.2010.04.004

Zheng, G. X., Terry, J. M., Belgrader, P., Ryvkin, P., Bent, Z. W., Wilson, R., . . . Bielas, J. H. (2017). Massively parallel digital transcriptional profiling of single cells. *Nat Commun*, *8*, 14049. doi:10.1038/ncomms14049

Zuberbuehler, M. K., Parker, M. E., Wheaton, J. D., Espinosa, J. R., Salzler, H. R., Park, E., & Ciofani, M. (2019). The transcription factor c-Maf is essential for the commitment of IL-17-producing gammadelta T cells. *Nat Immunol, 20*(1), 73-85. doi:10.1038/s41590-018-0274-0

Zwiener, I., Frisch, B., & Binder, H. (2014). Transforming RNA-Seq data to improve the performance of prognostic gene signatures. *PLoS One, 9*(1), e85150. doi:10.1371/journal.pone.0085150

Figures

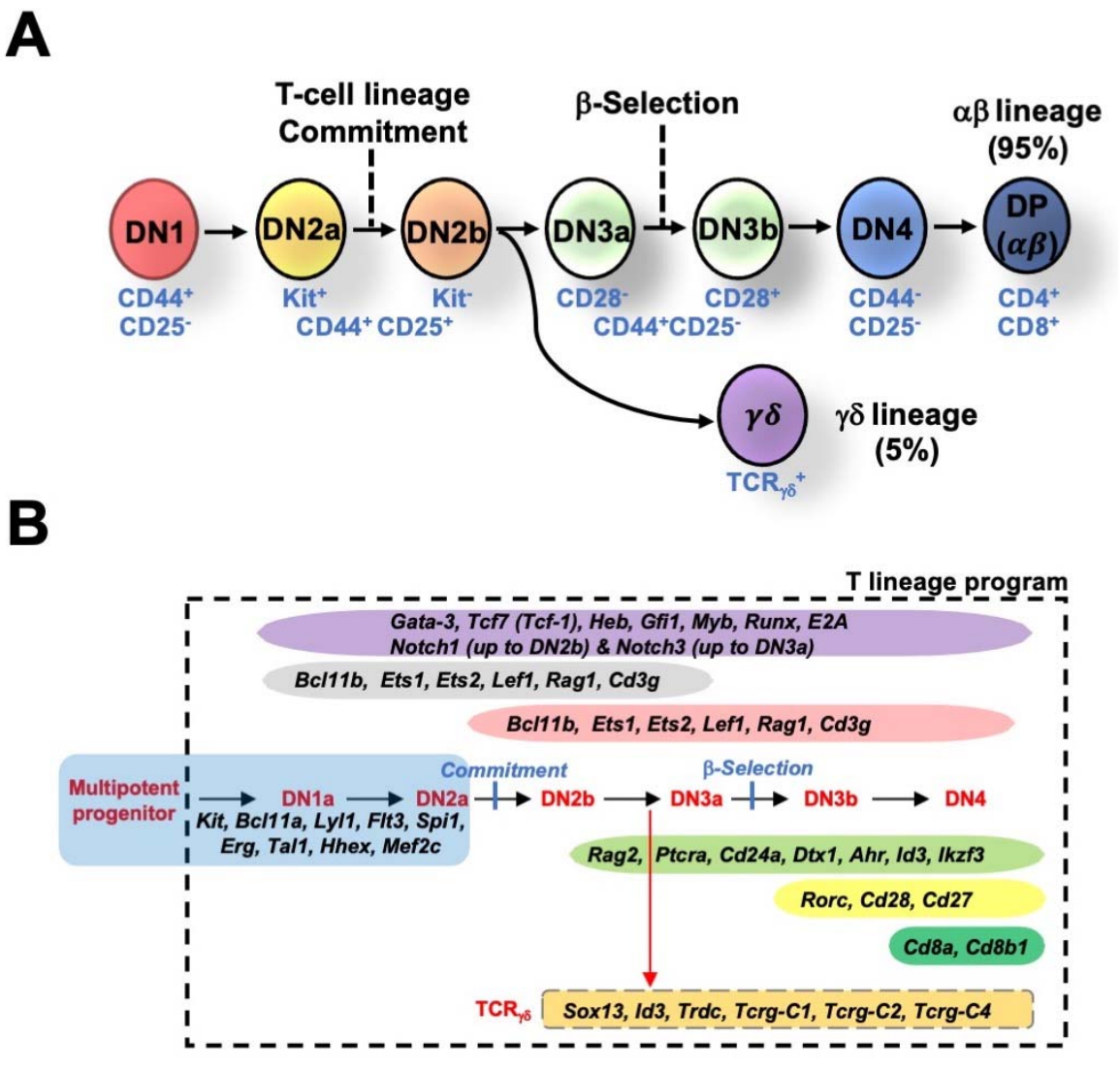

Fig EV1 - The current model of murine T cell development.

A T cells are divided into two main lineages, αβ and γδ T cells, which are defined by T cell receptor (TCR) chain expression. Shown is a schematic overview of early T cell development. These earliest stages in the thymus are divided into four stages, termed double negative (DN) 1 to 4, based on expression of key cell surface markers.

B The key markers are indicated. The current model assumes the γδ lineage branches off from αβ lineage during DN2b>DN3a stage, when *TCRB/G/D* gene rearrangements occur. Also shown is a summary of the expression patterns of key marker genes that define the DN stages of T cell development as define at a population level.

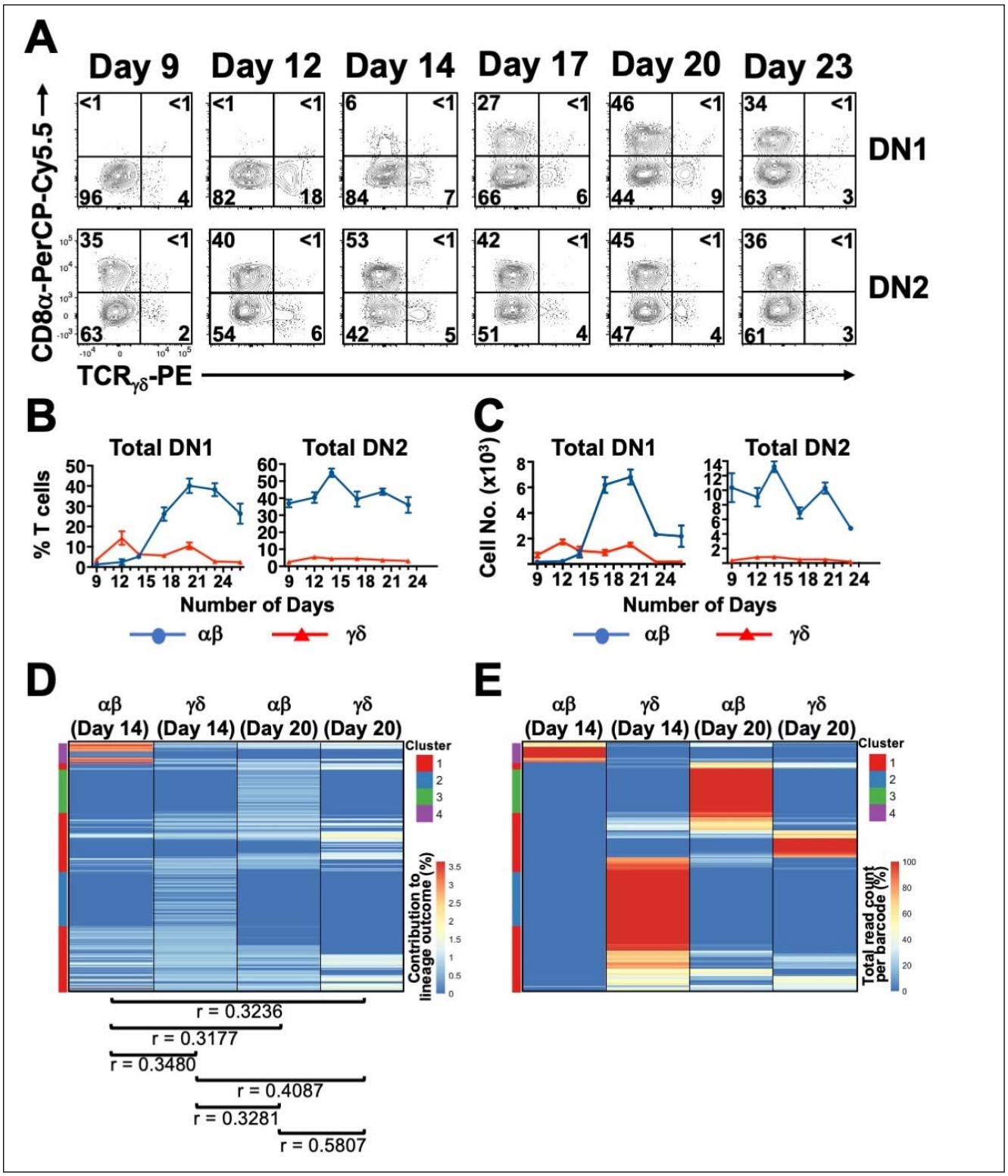

Figure 1. Potential heterogeneity in the lineage outcomes of DN1 thymocytes.

A Total DN1 ($CD44^+CD25^-Lin^-$) and DN2 ($CD44^+CD25^+Lin^-$) thymocytes were sorted from the thymus of C57BL/6 mice then analyzed for αβ versus γδ lineage outcomes in OP9-DL1 cultures. The cultures were analyzed at the indicated time points by flow cytometry. αβ lineage cells were identified as $CD8\alpha^+$ while γδ lineage cells were identified as $TCR\gamma\delta^+$. CD4 expression was also analyzed but was concomitant

with CD8α expression (not shown). Lin = CD4, CD8, B220, CD11b and CD11c. Representative flow cytometric plots are shown.

B The mean percentages ± S.E.M. of 4 to 7 replicates are shown. **(c)** The mean cell numbers ± S.E.M. are shown.

C, D Barcoded total DN1 thymocytes were differentiated on OP9-DL1 cells. αβ and γδ cells were then sorted from the culture at 14d and remaining culture was sorted at 20d. The barcode composition of the four populations was then analyzed. Heatmaps are comparing by individual barcodes (rows) across the four populations the (column) are shown.

E Heatmap with normalization of barcodes within each population is shown in **(D)**, while normalization of each barcode usage across all four populations is shown in **(E)**. Indicated under **(D)** are Pearson's correlation (*r*) analysis between each pair of populations. Shown is one replicate of two independent experiments. The second replicate is shown in Fig EV2C-D and the corresponding t-SNE clustering to group the barcodes information is shown in the Fig EV2B.

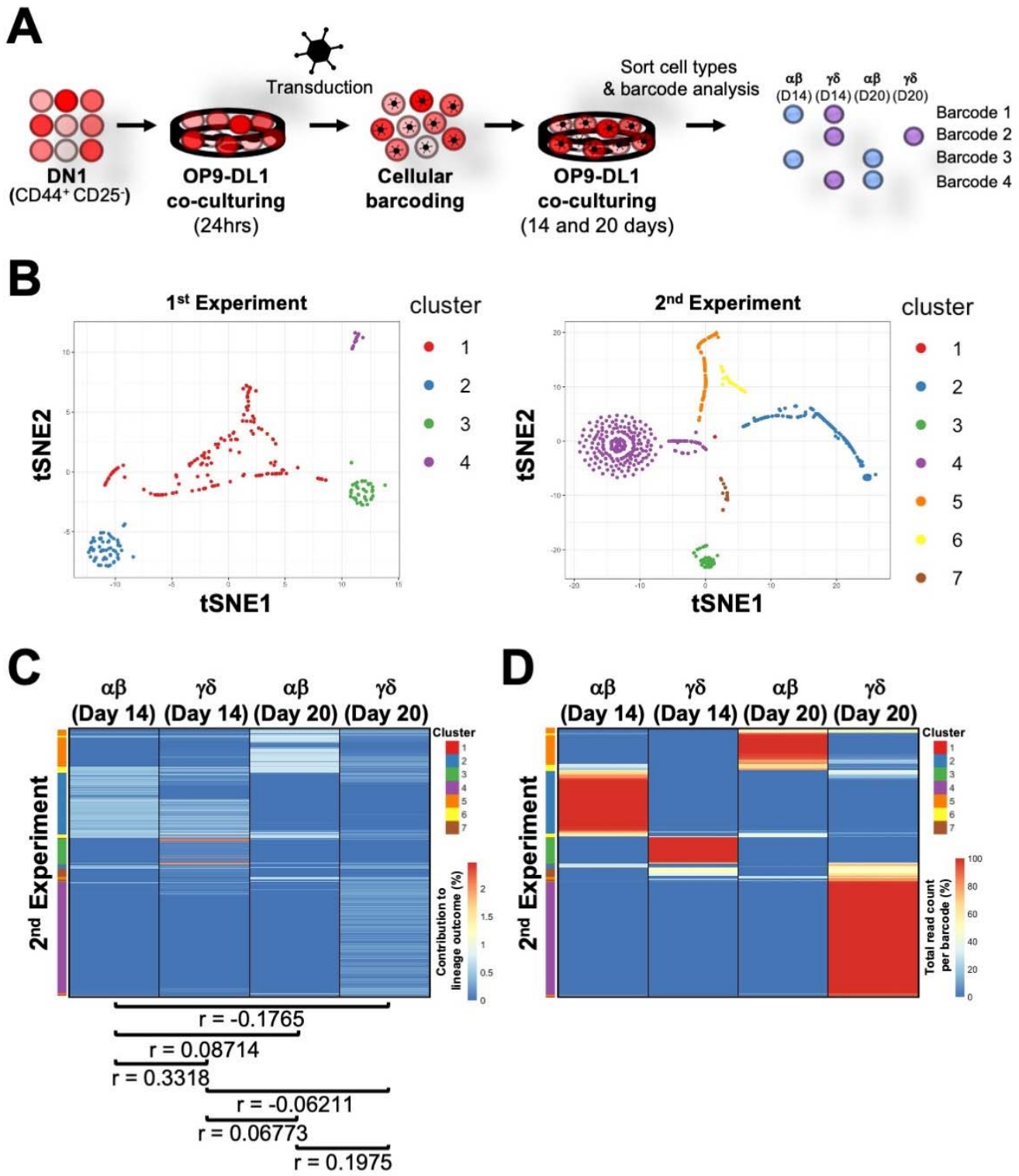

Figure EV2. Cellular barcoding to track lineage outcomes of individual DN1 thymocytes.

A Schematic overview of experimental set up of cellular barcoding. Total DN1 ($CD25^{+}CD44^{+}$) thymocytes sorted from the thymus of C57BL/6 mice were pre-cultured on OP9-DL1 for 24h. Cells were tagged with unique genetic heritable cellular barcodes by transduction with lentiviral library of the barcode. The results in inheritance of tags in the daughter cells derived from the transduced DN1 thymocytes. Half the culture was then

sorted at 14d for αβ (CD90.2^{+} CD8a^{+} TCRγδ^{-}) and γδ (CD90.2^{+} CD8a^{+} TCRγδ^{-}) lineage cells. The remaining half was then sorted for αβ and γδ cell lineage cells at 20d. Barcode composition of the four populations was then analyzed by PCR and Illumina sequencing.

B DBSCAN clustering was performed on barcoded cells to group cells based on their distinct barcode usage. The left plot shows the first experiment, while the right plot shows the second experiment. Shown are the t-SNE outputs. These cluster were used to generate heatmaps from Fig 1D and 1E and Fig EV2C-D.

C, D Analysis of barcode composition of the four sorted populations from differentiating DN1 thymocytes in OP9-DL1 cocultures. Shown is a replicate of the experiments of that presented in Fig 1D and 1E. Heatmaps are comparing by individual barcodes (rows) across the four populations the (column) are shown. Heatmap with normalization of barcodes within each population is shown in **(C)**, while normalization of each barcode usage across all four populations is shown in **(D)**. Indicated under **(C)** are Pearson's correlation (*r*) analysis between each pair of populations.

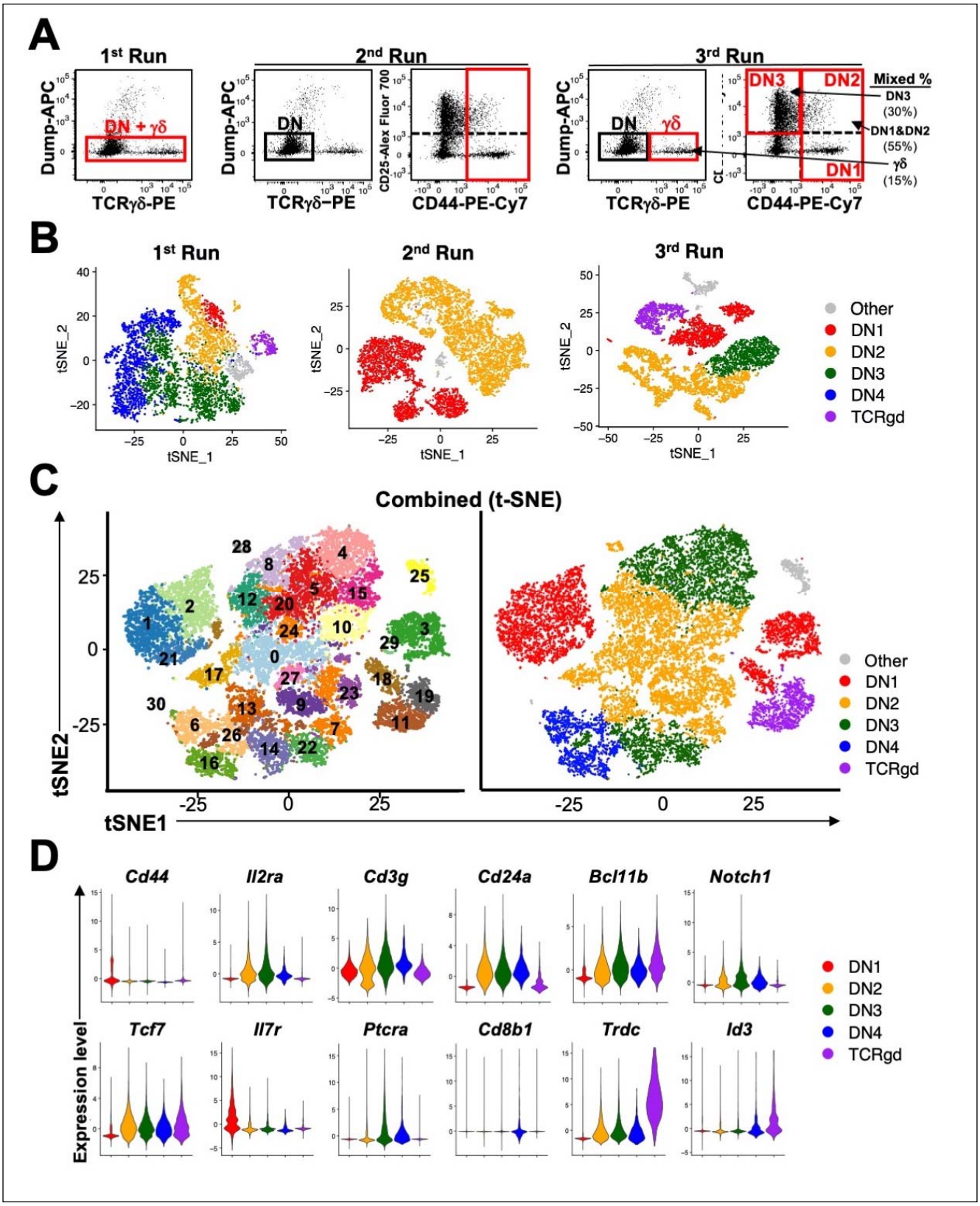

Figure 2. Single-cell RNA sequencing analysis of early T cell development.

A Shown are the gating strategies used to sort DN and γδ thymocytes from C57BL/6 mice for 10X scRNA-seq. Three separate runs were completed. The first run was on total DN and TCRγδ^{+} cells. The

second run was on only DN1 and DN2 cells. The third run involved sorting DN1 plus DN2, DN3 and TCRγδ$^+$ cells separately, which were then mixed back together post-sort at a ratio of 55% to 30% to 15% respectively. Dump = CD4, CD8, B220, CD11b, CD11c and TCRβ.

B Following processing of the 10X data on CellRanger, each dataset was analyzed for clustering based on the first 12 principal components in Seurat. Shown is the t-SNE plot of each run color-coded to DN developmental stage, TCRγδ$^+$ thymocytes or other (non-thymocytes).

C The three datasets, totaling 22,094 cells, were integrated with SCTransform, then clustered with Seurat. This yielded 30 distinct clusters (left plot), which were then annotated to DN developmental stage, TCRγδ$^+$ thymocytes or other (non-thymocytes) (right plot).

D Violin plots showing expression of selected markers used to assign individual clusters to DN development stage.

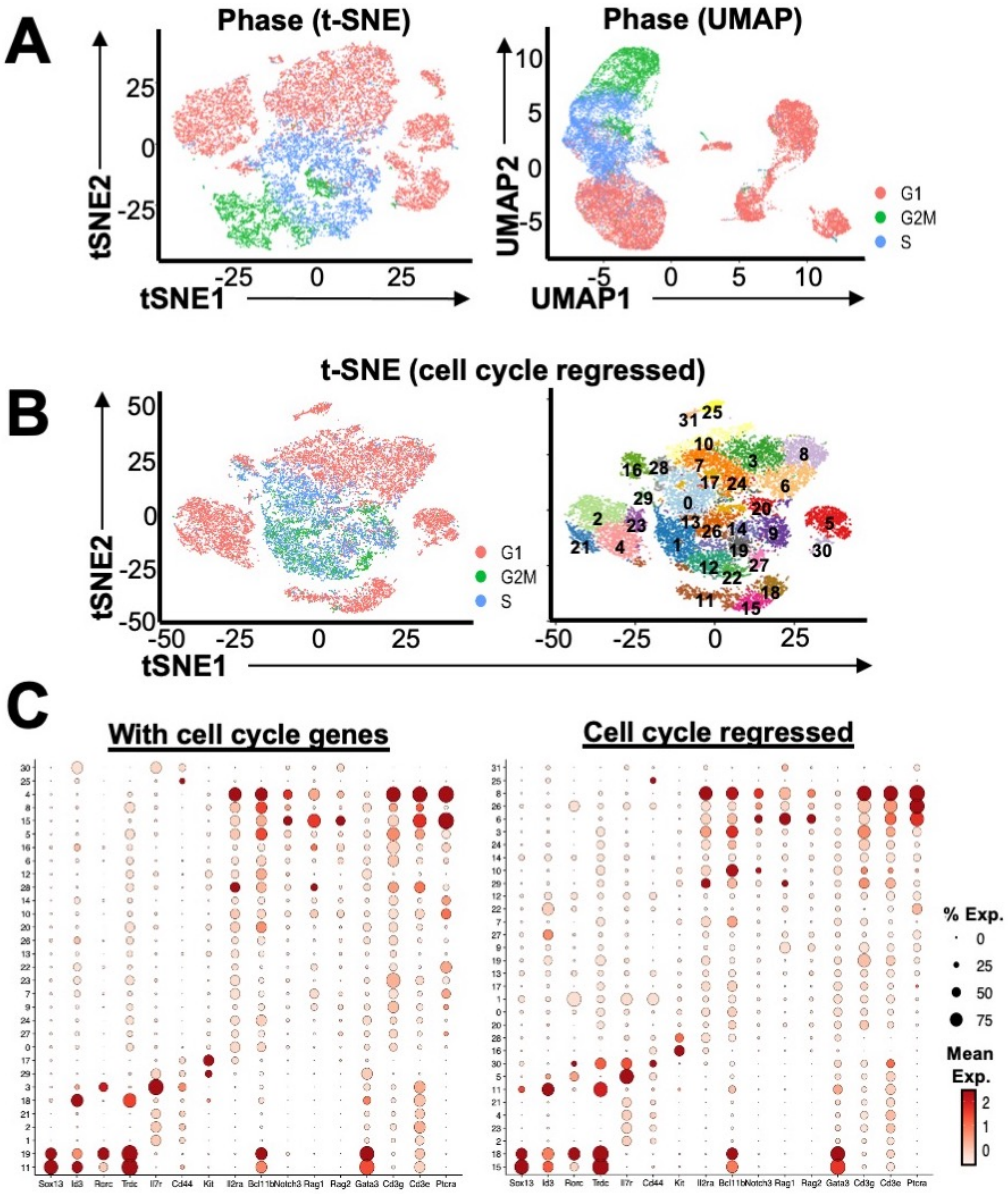

Figure EV3. Cell cycle has a minimal to the clustering of the DN thymocyte scRNA-seq data.

A t-SNE (left) and UMAP (right) visualization of the integrated scRNA-seq data derived from the three 10X runs of DN and TCRgd^{+} thymocytes. Each cell was tagged as in G1, G2M or S stage of the cell cycle based on expression of cell cycle genes.

B Cell cycle genes were first regressed out using Seurat's built-in regression model and clustered. The cells were then retagged to cell cycle stage (left). 31 distinct clusters were resolved (right).

C Dot plot showing the expression of key markers genes across the clusters comparing with cell cycle genes left in or regressed out. Dot size indicates the percentage of cells in each cluster expressing the gene, while color saturation indicates average expression level of the cluster.

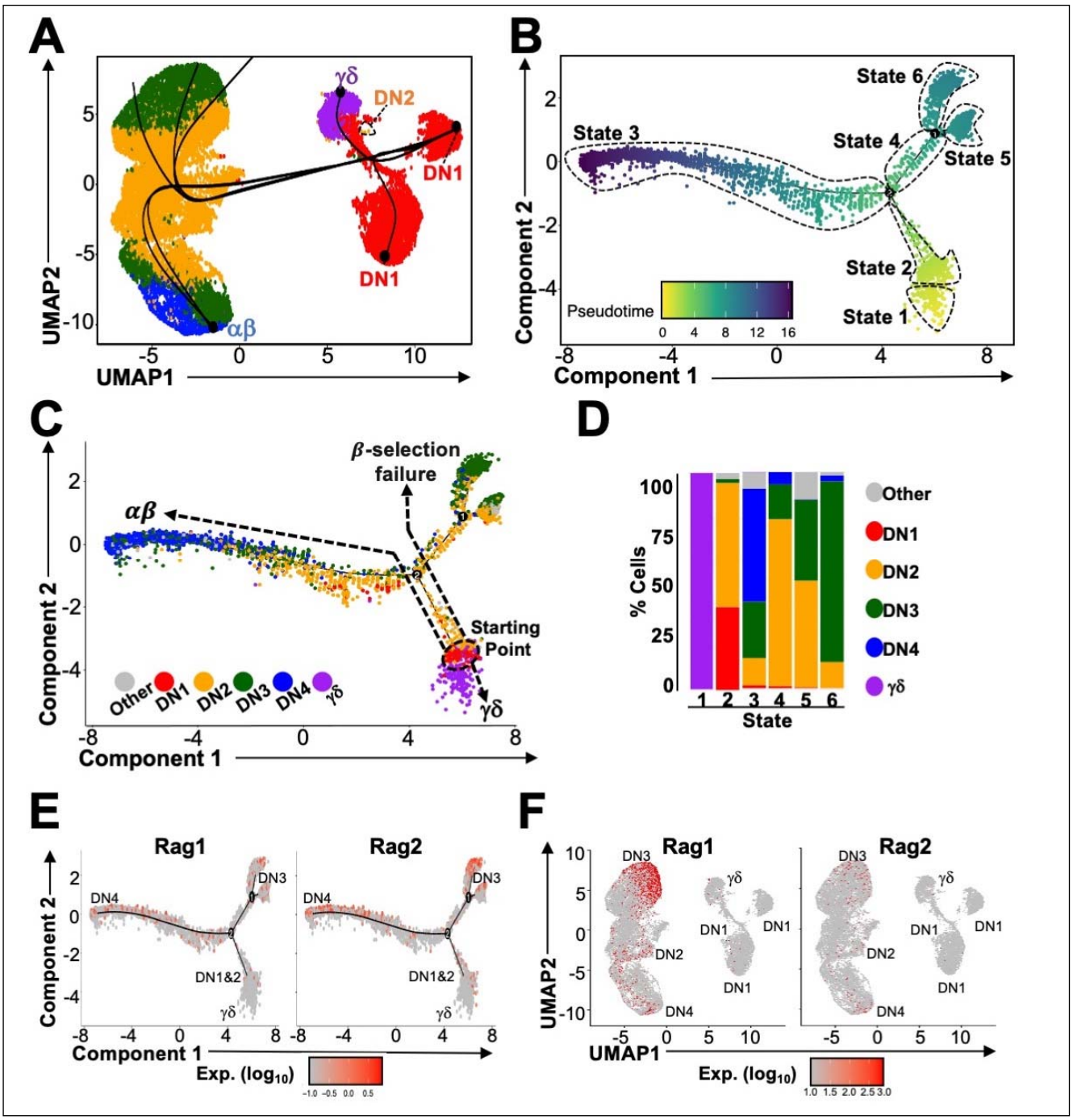

Figure 3. Trajectory analyses predict αβ and γδ T cell development occurs in parallel from the DN1 stage.

A Pseudotime analysis of the integrated 10X dataset with Slingshot (visualized by UMAP), which predicts the progression from DN1 to DN4 (αβ lineage) and γδ T cells based in transcriptional profiles. Cells are color-coded by developmental stage.

B Pseudotime analysis of total DN and γδ thymocytes (first 10X run) with Monocle 2. The six states identified in the asymmetric trajectory are indicated.

C Color-coding of the Monocle 2 analysis by thymocyte development stage based on expression of marker genes by the individual clusters.

D Shown are the proportions of DN developmental stage or TCR$\gamma\delta^+$ cells that contributed to each state of the Monocle 2 analysis.

E Expression of *Rag1* and *Rag2* overlaid onto the Monocle 2 analysis.

F Expression of *Rag1* and *Rag2* overlaid onto the Slingshot analysis.

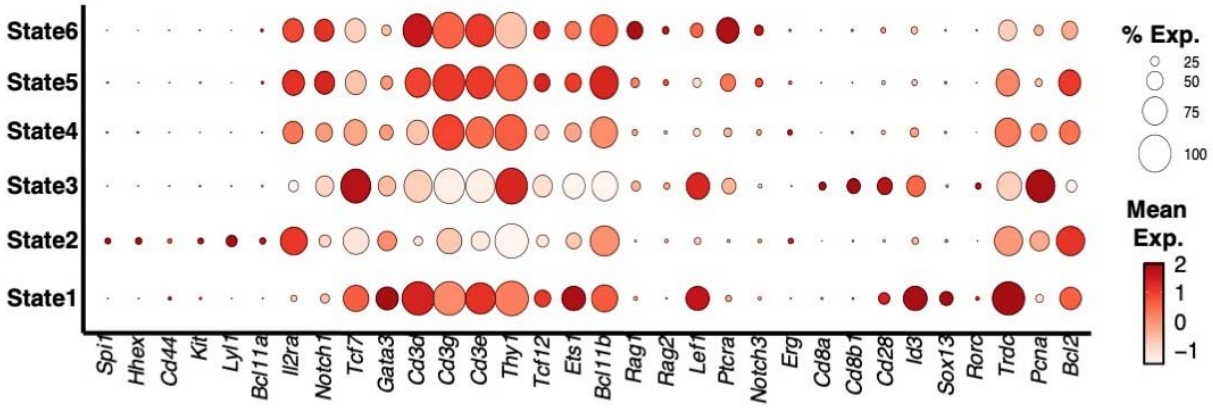

Figure EV4. Assessment of the states inferred by Monocle 2 trajectory analysis of total DN and γδ thymocytes.

Dot plot showing the expression of key canonical markers across the six states identified from the pseudotime inference by Monocle 2 in Fig 3B-D. Dot size indicates the percentage of cells in each state expressing, while color saturation indicates average expression level within the state.

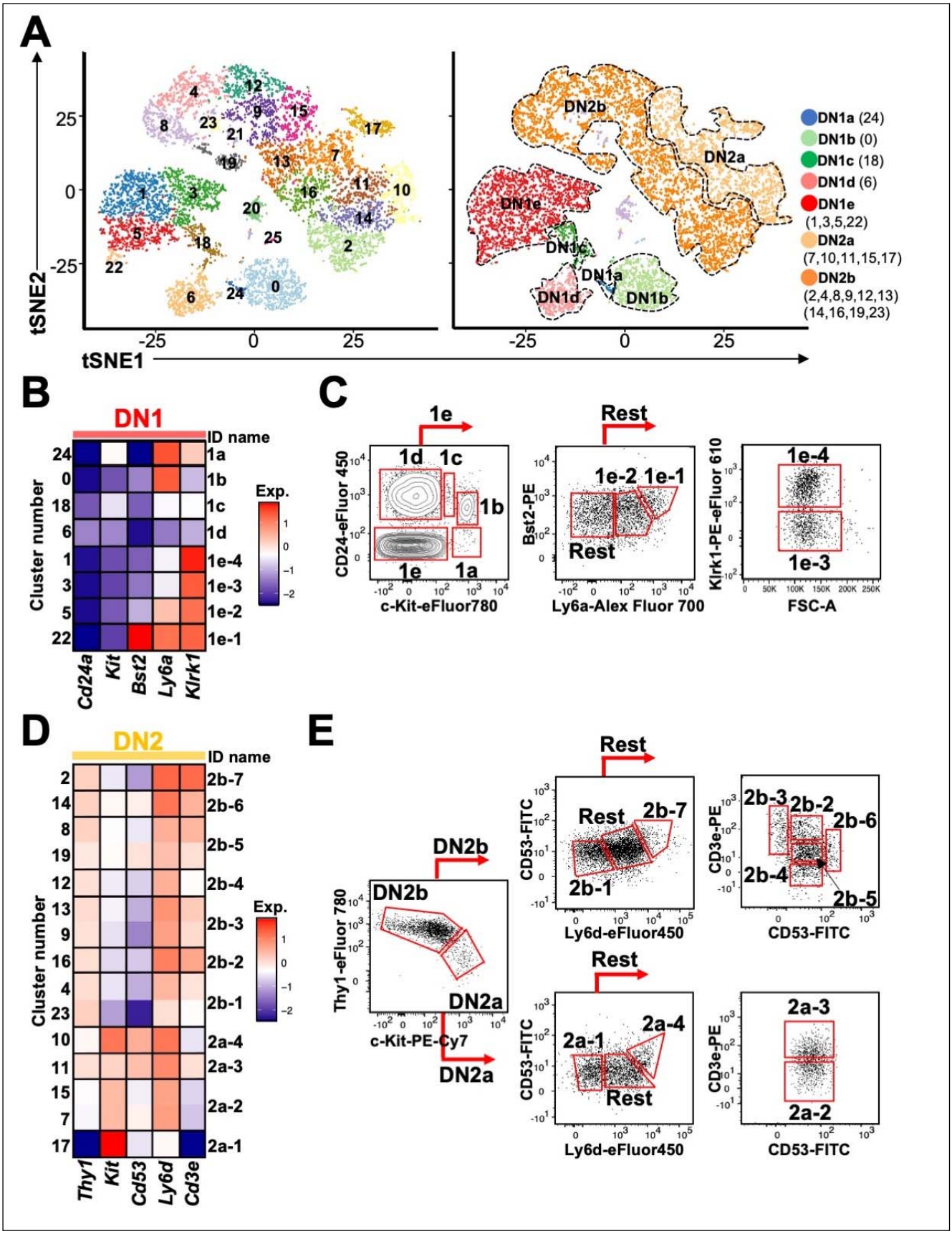

Figure 4. Identification of cell surface markers for delineating DN1 and DN2 the subpopulations inferred from scRNA-seq.

A t-SNE visualization of 8,851 DN1 and DN2 thymocytes from the second 10X run clustered with Seurat. This yielded 26 distinct clusters (left plot), which were then annotated as DN1a, DN1b, DN1c, DN1d, DN1e, DN2a or DN2b (right plot).

B Genes found to be differentially expressed between DN1 subpopulations were annotated against Gene Ontology (GO) terms for cell surface markers (Appendix Fig S1). Shown is a heatmap showing the average expression of the genes encoding cell surface proteins selected to delineate the DN1 subpopulations.

C Flow cytometric validation of the selected markers used to identify DN1 subpopulations. Total DN1 cells ($CD4^-CD8^-$ $CD44^+CD25^-Lin^-$) were first divided into five populations based on c-Kit and CD24. The c-Kit^-CD24^- cells (total DN1e) was then divided into three populations based on Ly6a and Bst2. Finally, the $Ly6a^-Bst2^-$ cells were divided into two populations based on Klrk1. Lin = B220, CD11b, CD11c, TCRβ and TCRγδ.

D Heatmap showing the average expression of genes encoding cell surface proteins selected to delineate the DN2 subpopulations.

E Flow cytometric validation of the selected markers used to identify DN2 subpopulations. Total DN2 cells ($CD4^-CD8^-$ $CD44^+CD25^+Lin^-$) were first divided into two populations based on c-Kit and Thy1. The c-Kit^+Thy1^{int} cells (total DN2a) were divided into three populations based on Ly6d and CD53. Then, the c-$Kit^+Thy1^{int}Ly6d^{int}CD53^-$ cells were divided into two populations based on CD53 and CD3e. The c-Kit^- $Thy1^+$ cells (total DN2b) were divided into three populations based on Ly6d and CD53. Then, the c-$Kit^+Thy1^{int}Ly6d^{int}CD53^{int/+}$ cells were divided into five populations based on CD53 and CD3e.

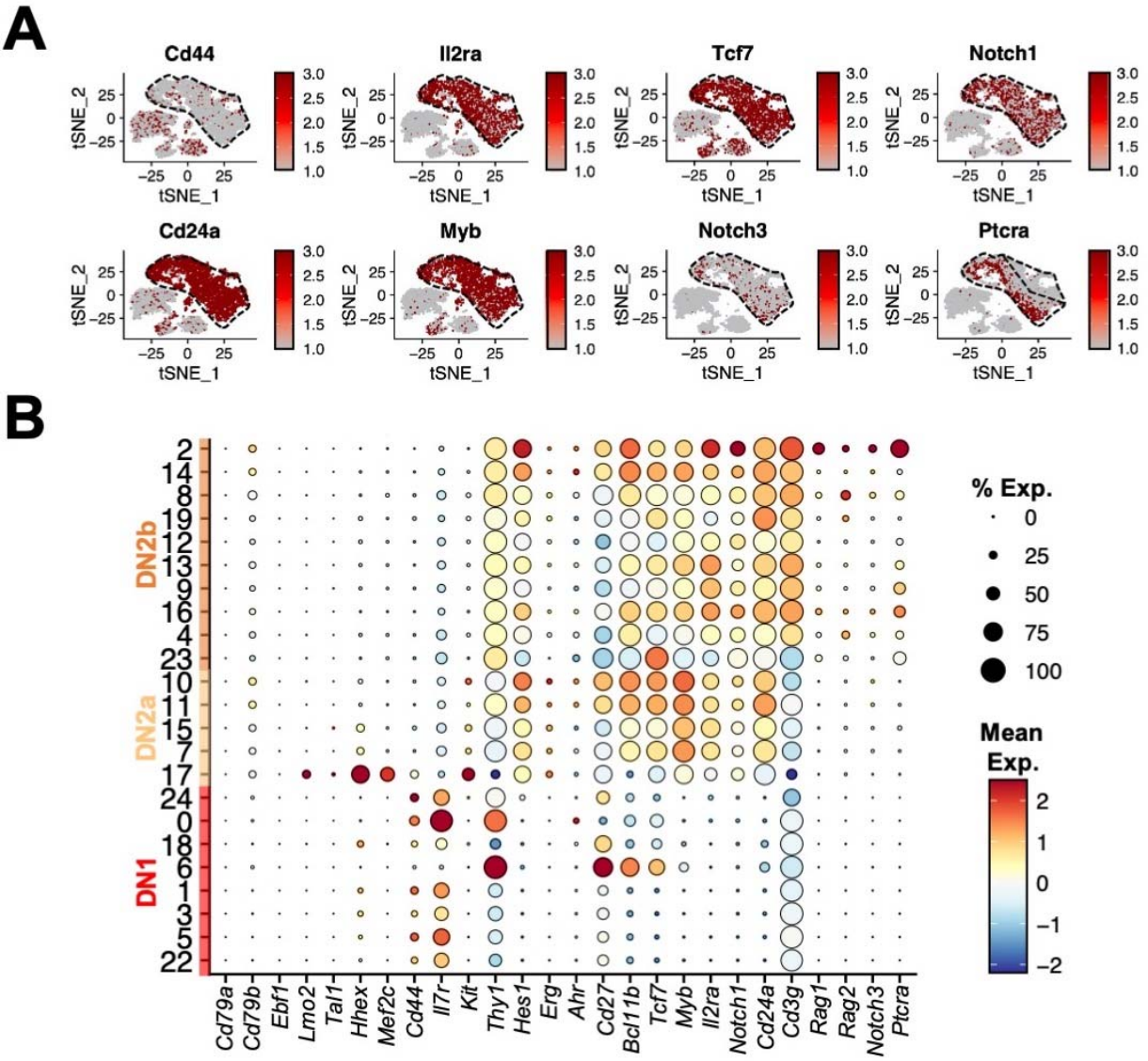

Figure EV5. Single-cell analysis reveals extensive heterogeneity within DN1 and DN2 thymocytes.

A Feature plots of some of the markers used to define the clusters in Fig 4A.

B Dot plot showing the expression of key markers previously shown to be differentially expressed between DN1, DN2a and DN2b. Cluster 20, 21 and 25 identified as other cells (doublets and B cells) were removed for simplicity. Dot size indicates the percentage of each cluster expressing the gene (% Exp.), and color saturation represents the strength of average expression.

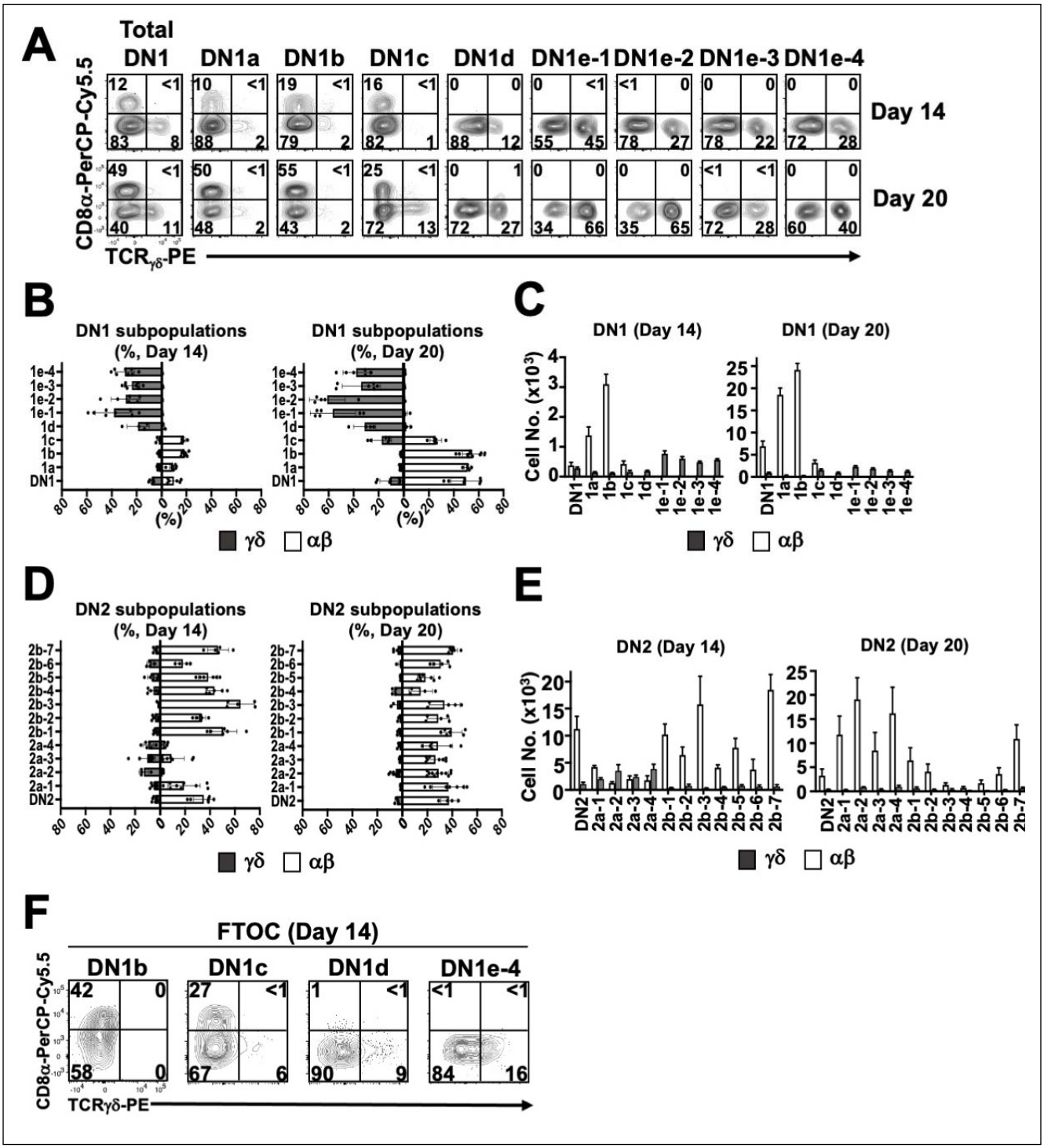

Figure 5. Analyzing the αβ or γδ potential of DN1 subpopulations.

A Sorted DN1 subpopulations were cultured on OP9-DL1 cells to assess their lineage potential. The cultures were analyzed at 14d and 20d of culture by flow cytometry. αβ lineage cells were identified as $CD8\alpha^+$ while γδ lineage cells were identified as $TCR\gamma\delta^+$. Representative flow cytometric plots are shown. **B, C** Pooled data analyzing αβ versus γδ differentiation from sorted DN1 subpopulations. The means ±

S.E.M. of four to nine replicates performed over four independent experiments are shown. See Appendix Table S2 and S3 for *P*-value calculations.

D, E Pooled data analyzing αβ versus γδ differentiation from sorted DN2 subpopulations. The means ± S.E.M. of four to nine replicates performed over four independent experiments are shown. See Appendix Table 4 and 5 for *P*-value calculations.

F Repopulation of dGuo-depleted fetal FTOCs with select DN1 subpopulations. The lobes were then analyzed by flow cytometry for CD8α versus TCRγδ expression after 14d. Shown is a representative from three independent experiments.

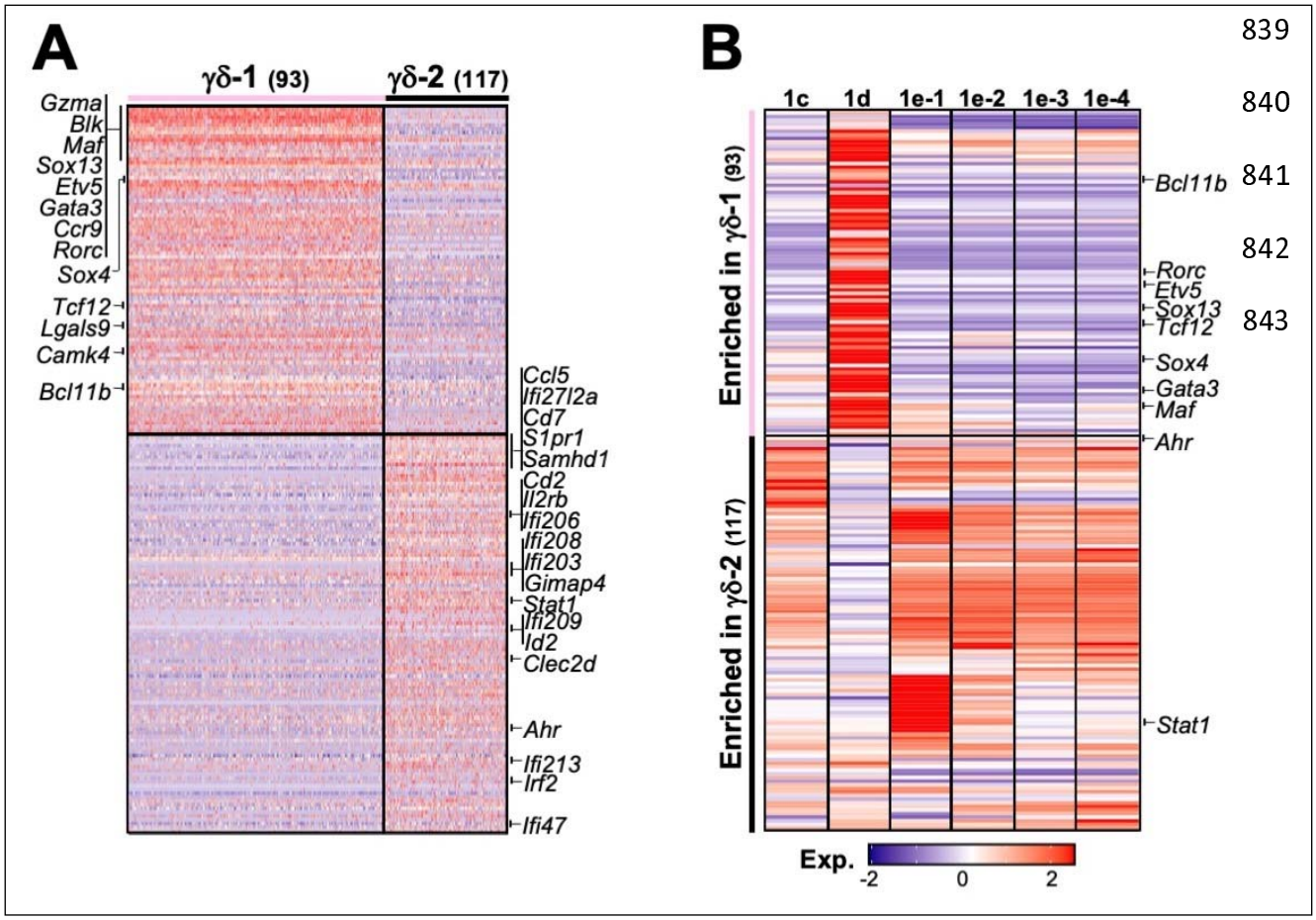

Figure 6. The gene expression profiles of the different DN1 subpopulations correlate with distinct γδ effector subsets.

A Heatmap showing genes differentially expressed (*P*-value <0.05 and 2-fold difference) between the γδ-1 and γδ-2 thymocyte subpopulations identified in the cluster analysis (clusters 11 and 19) of DN and γδ

thymocyte scRNA-seq data from Figure 2c. Each column is an individual cell in the dataset while each row is a differentially expressed gene. Genes associated with either IL-17A (left side) or IFNγ production (right side) are indicated.

B Analysis of DN1 subpopulations for expression of the 210 genes differentially expressed between the two γδ thymocyte populations. Transcription factors associated with either IL-17A or IFNγ are indicated.

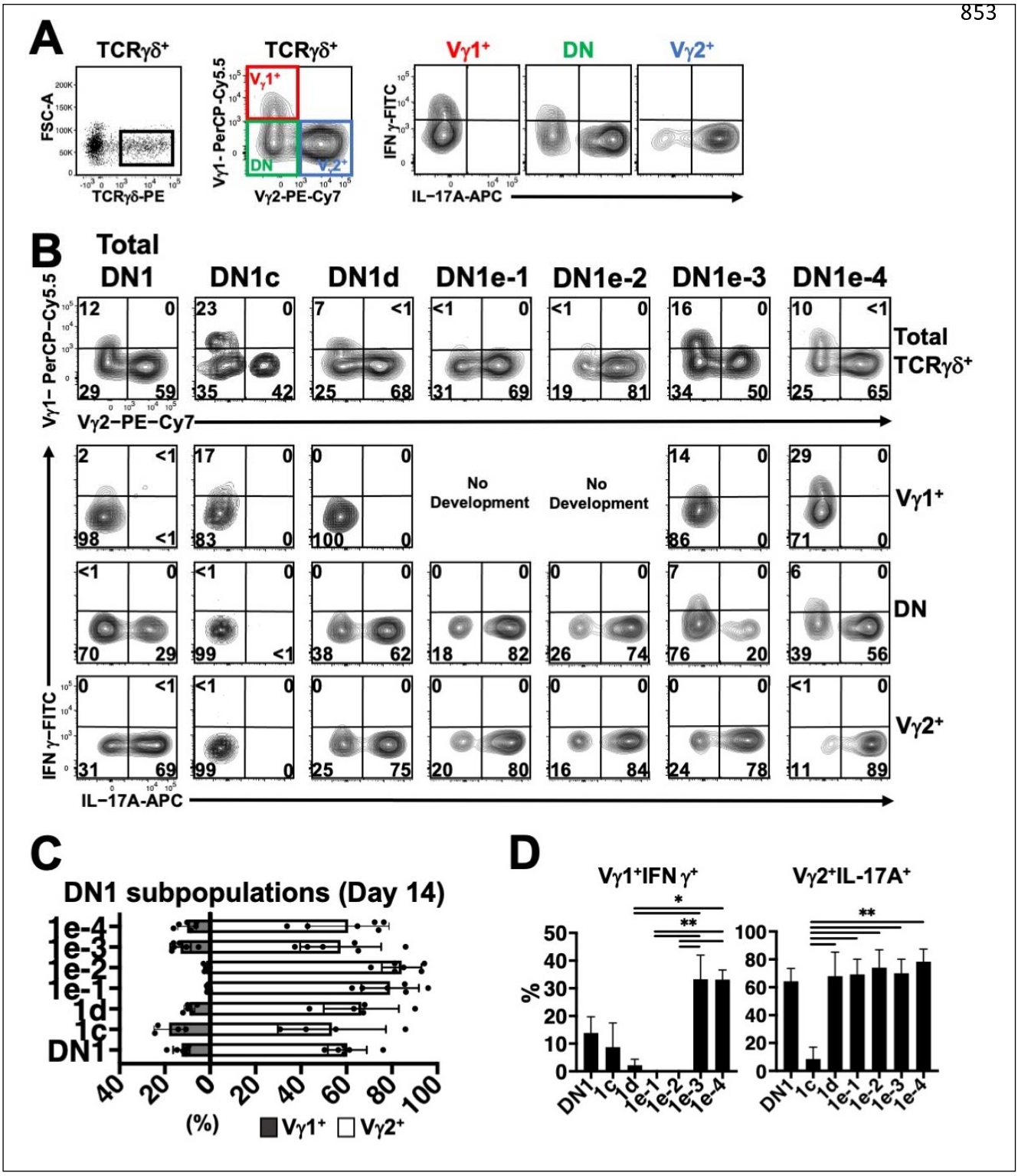

Figure 7. Analysis of γδ effector subset outcomes from DN1 subpopulations.

A Gating strategy for analyzing the phenotype of γδ T cells generated from DN1 subpopulations after co-culturing with OP9-DL1 cells for 14 days. TCRγδ^{+} (CD4^{-}CD8^{-}TCRβ^{-}) were first divided based on Vγ1 versus Vγ2 expression. The three subpopulations, including Vγ1^{-}Vγ2^{-} double negative (DN) cells were then analyzed for intracellular IL-17A and IFNγ expression.

B Shown are the flow cytometric plots from a representative of three independent experiments for cytokine expression by γδ T cells derived from DN1 subpopulations. The top row shows the Vγ1 versus Vγ2 expression. Gated $V\gamma1^+$, $V\gamma2^+$ and double negative (DN) cells were then analyzed for IL-17A versus IFNγ expression in the bottom three rows.

C Pooled data analyzing the percentage of Vγ1 versus Vγ2 cells differentiated from sorted DN1 subpopulations. The means ± S.E.M of four to six replicates performed over three independent experiments is shown. See Appendix Table S6 for *P*-value calculations.

D Pooled data analyzing percentage of $V\gamma1^+IFN\gamma^+$ (left) and $V\gamma2^+IL\text{-}17A^+$ (right) cells out of total $TCR\gamma\delta^+$ cells. The means ± S.E.M is shown (**P*<0.05, ***P*<0.01).